Maternal hepatic adaptations during obese pregnancy encompass lobe-specific mitochondrial alterations and oxidative stress

Luís F. Grilo (1,2), luis.grilo@uc.pt

ORCID: 0000-0002-6278-9241

João D. Martins (1), jdgmartins@gmail.com

ORCID: 0000-0003-3676-3053

Mariana S. Diniz (1), marianasdiniz.diniz@gmail.com

ORCID: 0000-0002-2161-9676

Carolina Tocantins (1), carolina.tocantins.23.3@gmail.com

ORCID: 0000-0002-3758-0454

Chiara H. Cavallaro (1), chi.cavallaro@gmail.com

ORCID: NA

Inês Baldeiras (3), ines.baldeiras@sapo.pt

ORCID: 0000-0002-8106-7308

Teresa Cunha-Oliveira (1), teresa.oliveira@gmail.com

ORCID: 0000-0002-7382-0339

Stephen Ford (4), SPFord@uwyo.edu

ORCID: NA

Peter W. Nathanielsz (4), peter.nathanielsz@uwyo.edu

ORCID: 0000-0001-8410-6280

Paulo J. Oliveira (1), pauloliv@cnc.uc.pt

ORCID: 0000-0002-5201-9948

Susana P. Pereira (1,5), pereirasusan@gmail.com

ORCID: 0000-0002-1168-2444

1- CNC - Center for Neuroscience and Cell Biology, CIBB - Centre for Innovative Biomedicine and Biotechnology, University of Coimbra, UC-Biotech, Biocant Park, Cantanhede, Portugal

2 - Ph.D. Programme in Experimental Biology and Biomedicine (PDBEB), Institute for Interdisciplinary Research (IIIUC), University of Coimbra, Coimbra, Portugal

3-Neurological Clinic, Faculty of Medicine, University of Coimbra, Coimbra, Portugal

4 - Department of Animal Science, University of Wyoming, Laramie, WY, USA

5 - Laboratory of Metabolism and Exercise (LametEx), Research Centre in Physical Activity, Health and Leisure (CIAFEL), Laboratory for Integrative and Translational Research in Population Health (ITR), Faculty of Sport, University of Porto, Porto, Portugal

Keywords: gestation; maternal malnutrition; overnutrition; liver disease; hepatic mitochondria

Corresponding author: Susana P. Pereira, PhD

CNC-Center for Neuroscience and Cell Biology, UC Biotech, Biocant Park, University of Coimbra, 3060-197 Cantanhede, PORTUGAL

phone: +351-231-249-170,

fax: +351-239-853-409,

email: pereirasusan@gmail.com

ORCID: 0000-0002-1168-2444

Funding

Funded by ERDF funds through the Operational Programme Competitiveness Factors – COMPETE2020 and national funds by Foundation for Science and Technology under FCT-Post-doctoral Fellowship (SPP, SFRH/BPD/116061/2016), FCT-doctoral Fellowship (LFG, SFRH/BD/5539/2020; MSD, SFRH/BD/11934/2022; CT, SFRH/BD/11924/2022), LFG, CT, and MSD were supported by the project “Summer Course in Interdisciplinary Research, Development and Innovation in Cellular and Molecular Metabolism” (15-20/7/245), funded by

the FCT and Directorate General for Higher Education (DGES), project grant PTDC/DTP-DES/1082/2014(POCI-01-0145-FEDER-016657), CENTRO-01-0246-FEDER-000010 (Multidisciplinary Institute of Ageing in Coimbra) strategic project UIDB/04539/2020, UIDP/04539/2020, LA/P/0058/2020 and NIH grant R01HD070096-01A1.It was also funded by the European Union (HORIZON-HLTH-2022-STAYHLTH-101080329). Views and opinions expressed are however these of the author(s) only and do not necessary reflect those of the European Union or the Health and Digital Executive Agency. Neither the European Union nor the granting authority can be held responsible for them.The funding agencies had no role in study design, data collection and analysis, decision to publish, or preparation of this document. There are no conflicts of interest associated with this work.

Abstract

Maternal obesity(MO) is rising worldwide, affecting half of all gestations, constituting a possible risk-factor for some pregnancy-associated liver diseases (PALD) and hepatic diseases. PALD occur in approximately 3% of pregnancies and are characterized by maternal hepatic oxidative stress (OS) and mitochondrial dysfunction. Maternal hepatic disease increases maternal and fetal morbidity and mortality. Understanding the role of MO on liver function and pathophysiology could be crucial for better understanding the altered pathways leading to PALD and liver disease, possibly paving the way to prevention and adequate management of disease. We investigated specific hepatic metabolic alterations in mitochondria and oxidative stress during MO at late-gestation.

Maternal hepatic tissue was collected at 90% gestation in Control and MO ewes, which fed 150% of recommended nutrition starting 60 days before conception. Maternal hepatic redox state, mitochondrial Respiratory Chain (MRC) and OS markers were investigated. MO decreased MRC complex-II activity and its subunits SDHA and SDHB protein expression, increased complex-I and complex-IV activities despite reduced complex-IV subunit mtCO1 protein expression, and increased ATP synthase ATP5a subunit. Hepatic MO-metabolic remodeling was characterized by decreased ANT-1/2 and VDAC protein expression and PKA activity ($p<0.01$), and augmented NAD+/NADH ratio due to reduced NADH levels ($p<0.01$). MO showed an altered redox state with increased OS, increased lipid peroxidation ($p<0.01$), decreased GSH/GSSG ratio ($p=0.005$), increased SOD($p=0.03$) and decreased catalase ($p=0.03$) antioxidant enzymatic activities, lower catalase, glutathione peroxidase (Gpx)-4 and glutathione reductase protein expression ($p<0.05$), and increased Gpx-1 abundance ($p=0.03$). MO-related hepatic changes were more evident in the right lobe, corroborated by the integrative data analysis.

Hepatic tissue from obese pregnant ewes showed alterations in the redox state, consistent with OS and MRC and metabolism remodeling. These are hallmarks of PALD and

hepatic disease, supporting MO as a risk-factor and highlighting OS and mitochondrial dysfunction as mechanisms responsible for liver disease predisposition.

Clinical Perspectives

- Previous epidemiological studies associated maternal obesity(MO) with increased maternal disease development during and after gestation, including some pregnancy-associated liver diseases(PALD) and liver disease. However, the cellular and molecular mechanisms underlying this association are poorly characterized.
- This work shows that MO during pregnancy results in altered maternal hepatic mitochondrial function and redox state, which potentially predisposes to hepatic dysfunction. Although a common effect of MO in both hepatic liver lobes exists, some of the differences observed are lobe-specific.
- Monitoring liver function during the challenging pregnancy period can provide new insights to understand and prevent complications in both the mother and offspring throughout/after gestation, while the found lobe distinct dysfunctions can be critical in liver disease diagnosis, biopsies analysis, and liver transplantation if extended to other hepatic pathologies.

Abbreviations

AFLP - Acute fatty liver pregnancy

ALT - Alanine Aminotransferase

BSA - Bovine Serum Albumin

C - Controls

complex III - Cytochrome c reductase

Complex-I - NADH dehydrogenase

complex-II - Succinate dehydrogenase

complex-IV - Cytochrome c oxidase

CS - Citrate Synthase

CytB - Cytochrome b

DHA - Docosahexaenoic acid

FAS - Fatty-Acid Synthase

FATP1 - Fatty-Acid Transport Protein 1

GPx - Glutathione peroxidase

GR - Glutathione reductase

GSH - Reduced Glutathione

GSSG - Oxidized Glutathione

HELLP syndrome - Hemolysis, elevated liver enzymes, low platelets syndrome

ICP - Intrahepatic cholestasis of pregnancy

LPL - Lipoprotein Lipase

MDA - Malondialdehyde

ML - Maternal liver

MLL - Maternal left liver lobe

MLR - Maternal right liver lobe

MO - Maternal obesity

MRC - Mitochondrial Respiratory Chain

NAFLD - Non-alcoholic fatty liver disease

NRC - National Research Council

OXPHOS - Oxidative phosphorylation system

PALD - Pregnancy-associated liver diseases

PCA - Principal Component Analysis

PKA - Protein Kinase A

PPAR - Peroxisome Proliferator-Activated Receptor

ROS - Reactive oxygen species

SREBP - Sterol Regulatory Element Binding Protein

YWHAZ - Tyrosine 3-monooxygenase/tryptophan 5-monooxygenase activation protein, zeta

Introduction

The incidence of obesity is rising exponentially worldwide among all age groups, including women of reproductive age[1]. More than 50% of pregnancies occur in overweight women[2]. Maternal obesity (MO) is associated with an increased risk of maternal (e.g., gestational diabetes, pre-eclampsia)[3], fetal (e.g., metabolic disease predisposition)[4], and pregnancy-related (e.g., abortion, stillbirth, postpartum hemorrhage)[3] comorbidities. MO can trigger maternal liver disease or exacerbate a pre-existing metabolic condition, leading to hepatic dysfunction throughout and/or after gestation[5].

The liver is crucial to maintain metabolic homeostasis throughout gestation-related increases in nutrient and energetic requirements[6]. During early pregnancy, the liver increases energy storage through triglyceride synthesis[7]. In late-gestation, hepatic fatty-acid oxidation increases to fulfill maternal energy requirements[7]. Pregnancy-associated liver diseases (PALD), including acute fatty liver pregnancy (AFLP), hemolysis, elevated liver enzymes, low platelets (HELLP) syndrome, and intrahepatic cholestasis of pregnancy (ICP). These clinical conditions are associated with higher morbidity and mortality rates and occur in up to 3% of pregnancies, Among PALD, obesity is considered a risk factor for HELLP syndrome and is a frequent comorbidity in women with ICP. Other reports also suggest that obesity, as well as being underweight, may be potential risk factors for ICP [6,8–11].

In rodents at 90% gestation (0.9G), MO induces an increase in maternal hepatic fat content, which positively correlates with protein abundance of Fatty-Acid Transport Protein 1 (FATP1), Peroxisome Proliferator-Activated Receptor (PPAR) γ, and Sterol Regulatory Element Binding Protein (SREBP)[12], accompanied with liver damage[13]. At 0.9G, but not 0.76G, maternal lipogenic Fatty-Acid Synthase (FAS) and Lipoprotein Lipase (LPL) protein expression were increased, whereas PPAR α protein abundance was decreased[14]. PPARα KO pregnant dams have increased circulating concentrations of serum fatty acids and their metabolites, including docosahexaenoic acid (DHA) and palmitate, and decreased β-hydroxybutyrate and lactate serum concentrations[15]. After birth, livers from obese mothers

show increased mono-unsaturated (omega-9/omega-7) fatty acids and decreased saturated and polyunsaturated (omega-3/omega-6) fatty acids concentrations[16], concomitantly with decreased plasma and hepatic C12 acylcarnitine levels[17]. Similar observations have been described in other hepatic metabolic diseases such as non-alcoholic fatty liver disease (NAFLD)[18,19], in which hepatic mitochondrial dysfunction and increased oxidative stress have been reported[20]. Systemic oxidative stress is observed even during healthy pregnancies[21]. AFLP is also related to mitochondrial dysfunction, usually associated with oxidative stress[22]. Increased liver inflammation, diffused hepatic steatosis, lower rough-surfaced endoplasmic reticula, dilated and swollen mitochondria, and broken mitochondrial cristae have been reported in HELLP syndrome[23].

Hepatic fibrosis and fat accumulation affect heterogeneously adult liver lobes in NAFLD[24–26]. Furthermore, hepatic drug distribution and uptake also appear to be lobe-dependent[27,28]. Different liver regions play different functions, a process called zonation[29]. Hepatocyte function differs depending on the distance to the closest blood supply, resulting from local oxygen tension variations[29]. Blood supply during fetal development is different between the fetal left and right lobes[30]. The right lobe presents lower pO_2 than the left lobe, resulting in functional cellular differences[31]. Other studies have revealed that hypoxia during fetal development results in epigenetic alterations, which change liver susceptibility to metabolic diseases in adulthood[32–34]. Together, these reports indicate potential lobe-dependent functional differences in the adult liver, contrasting with the prevailing idea that liver parenchyma was homogeneously functional throughout the solid organ.

We hypothesize that an obese mother's liver has an impaired ability to cope with the metabolic pregnancy challenge and that the burden of obesity during gestation can trigger hepatic metabolic imbalance with different impacts on the liver's right and left lobes. The contribution of MO- -related hepatic mitochondrial dysfunction and oxidative stress has not been explored as a trigger for post-gestational maternal liver disease. This study aimed to characterize and understand the MO-induced hepatic alterations in mitochondria- and oxidative stress-related mechanisms that occur during an obese pregnancy that can predispose to liver

disease development. Using a well-established MO sheep model[35] characterized by glucose metabolic impairment concomitant with increased glucose, insulin, and cortisol blood concentration at late gestation [36], we observed MO-induced lobe-dependent maternal hepatic mitochondrial dysfunction, increased oxidative damage, and impaired antioxidant enzymatic defense at late-gestation.

Materials and methods

Reagents

All of the used reagents were of the highest grade of purity available and all the aqueous solutions were prepared in ultrapure water (type I, Milli-Q Biocel A10 with pre-treatment via Elix 5, Millipore). For nonaqueous solutions, ethanol (99.5%, Sigma-Aldrich, Barcelona, Spain) or dimethyl sulfoxide (DMSO, Sigma-Aldrich) were used as solvents.

Table S1 lists all the reagents used in the present work, their suppliers, and commercial references.

Animal-related protocols

The animal cohort was performed at the University of Wyoming, Laramie, Wyoming, USA. All animal procedures were approved by the University of Wyoming Animal Use and Care Committee, and housed in facilities accredited by the Association for Assessment and Accreditation of Laboratory Animal Care International (protocol #20141022SF00126-01).

Eighteen nulliparous Western Rambouillet/Columbia ewes of similar morphological characteristics were randomly divided into two dietary groups. Ewes' adaption from their previous diet of mixed legume-grass hay to the experimental diet (Tables S2 and S3) was performed for one week. Were used healthy animals, without genetic modification or any previous procedure. All experimental animals were fed the necessary experimental diet to fulfill 100% of the National Research Council (NRC) nutritional recommendations during this period. After the adaptation period, the animals were randomly divided, grouped into six adjacent pens in an open-fronted pole barn, and fed according to the experimental groups. Controls (C; n=10 – an animal is an experimental unit) were fed a highly palatable diet that followed the NRC recommendations for nutrition[37]. This diet allows the maintenance of constant body weight and supports an increase of 10-15% in body weight during early gestation. The MO group (n=8) was fed 150% of NRC recommendations from sixty days before pregnancy, resulting in increased body weight as reported previously[35] (Figure 1A). The diets were maintained throughout gestation, adjusted for the body weight, and were entirely consumed. Ewes were fed

once daily at approximately 4 PM. The sample size was determined by the success of the conception of each sheep and the healthy pregnancy until 0.9G. Each group (C and MO) was divided into two pens per dietary treatment to allow replication. According to NRC guidelines, food amounts were individually calculated based on body weight and were adjusted weekly to account for body weight increases. An intact ram (white-faced, Rambouillet/Columbia breeding) bearing a marking harness was continuously maintained in each of the six pens for approximately six weeks, and on the first day each ewe was marked was considered day 0 of gestation (Figure 1A). Group allocation was known in every phase and used to better pair the samples during the experiments leading to the most reliable data. Total body weight was used to determine the ideal sample size.

Tissue collection

Maternal live weight was recorded. At 0.9G (between 132-140 days of pregnancy; normal pregnancy: ~150 days), ewes were sedated with Ketamine (22.2 mg/kg body weight) and maintained under isoflurane inhalation anesthesia (4% induction, 1-2% maintenance). Under anesthesia, ewes were exsanguinated, and the gravid uterus was quickly removed. The maternal liver was dissected, and tissue mass was determined. Maternal livers were divided into right and left lobes, snap-frozen in liquid nitrogen, and stored at -80°C for future use. All the samples were measured individually throughout all experiments.

Mitochondrial DNA copy number

Total DNA for mitochondrial DNA (mtDNA) copy number quantification was extracted from frozen liver tissue using the QIAamp DNA mini-kit (Qiagen, Düsseldorf, Germany), according to the manufacturer's instructions. Briefly, 20 mg of frozen liver tissue was weighed and incubated with digestion buffer and proteinase K at 56°C overnight. The obtained lysate was centrifuged, and the resulting supernatant was treated with RNase A. After incubation, the lysate was mixed with binding buffer and ethanol, and centrifuged through a silica-based spin column. Then, bound DNA was eluted by centrifuging elution buffer through the column. The

extracted DNA samples were quantified spectrophotometrically at 260 nm using a NanoDrop 2000 spectrophotometer (Thermo Scientific, Waltham, MA, USA), diluted to 20 ng/µL in extraction buffer, and stored at −20°C until use.

RT-PCR was performed using the SsoFast Eva Green Supermix, in a CFX96 real-time-PCR system (Bio-Rad, Hercules, CA, USA), with the primers defined in Table S4 at 500 nM. Amplification of 25 ng DNA was performed with an initial cycle of 2 min at 98°C, followed by 40 cycles of 5 seconds at 98°C plus 5 seconds at 63°C. At the end of each cycle, Eva Green fluorescence was recorded to enable the determination of Cq. After amplification, the melting temperature of the PCR products was determined by performing melting curves for quality control. For each set of primers, amplification efficiency was assessed, and no template controls were run. mtDNA copy number was determined in each sample by the ratio between the amount of the mitochondrial gene cytochrome b (CYTB) and the amount of the nuclear gene tyrosine 3-monooxygenase/tryptophan 5-monooxygenase activation protein, zeta (YWHAZ), using the CFX96 Manager software (v. 3.0; Bio-Rad).

Protein Quantification

After tissue homogenization, protein concentration in the lysates was determined using BioRad-DC protein assay from BioRad (Hercules, USA), according to the manufacturer's instructions. Briefly, this assay is based on the reaction of protein amino acids (primarily tyrosine and tryptophan, but also cystine, cysteine, and histidine) with an alkaline copper tartrate, followed by the reduction of a Folin substrate that leads to color development. After 15 minutes of reaction, the absorbance at 750 nm was measured using a Cytation 3 multi-mode microplate reader (BioTek Instruments, Inc.). Standard solutions containing 0.25 to 1.5 mg/mL Bovine Serum Albumin (BSA) were prepared using tissue homogenization buffer and used to infer the samples' protein concentration. Standards and samples were quantified using duplicates and triplicates, respectively.

Antioxidant enzymes activities

Catalase activity was determined by following hydrogen peroxide decomposition by measuring the 240 nm absorbance decrease. Tissue samples were resuspended in 50 mM Phosphate Buffer 50 mM, pH 7.8 (PB), and homogenized two times for 20 seconds with an UltraTurrax homogenizer from IKA (Staufen, Germany). Total tissue homogenates' volumes equivalent to 4 µg of total protein were diluted with 200 µL PB in a multi-well plate. The catalase activity assay was started by the addition of 100 µL hydrogen peroxide solution at 10 mM, as previously described[38]. The 240 nm absorbance was read every 15 seconds for 3 minutes at 25°C using the Cytation 3 multi-mode microplate reader (BioTek Instruments, Inc.). Purified catalase was used as a positive control. For each sample, separate wells containing the catalase inhibitor sodium azide were used as negative controls. Samples were measured in triplicates and negative controls were in duplicates. The first seven absorbance readings in each sample and respective controls were fitted to an one-phase-decay curve. The maximal catalase activity was determined using the initial linear part of this fitting curve. Results are expressed in enzyme units (U) obtained directly from the decomposition of hydrogen peroxide using the Beer-Lambert law with $l = 0.691$ cm and $\varepsilon = 43.6\ M^{-1}.cm^{-1}$.

For Glutathione peroxidase (GPx) and Glutathione Reductase (GR) activities, liver samples were minced with a scalpel on an ice-cold board and repeatedly washed with cold PBS until almost all the blood clots and other debris were removed. Then all the samples were homogenized in 800 µL PBS in a pre-cooled Potter Elvehjem glass homogenizer using a tight-fitting Teflon pestle (wall clearance: 0.10 mm) attached to a mechanical overhead stirrer (Heidolph, Schwabach, Germany) set to 600 rpm for 50-60 strokes. The samples were centrifuged at 250 g for 2 min at 4°C. The supernatants were collected and stored at -80°C.

GPx and GR activities were performed as described previously[39]. GPx activity was evaluated by spectrophotometry, using tert-butylperoxide as substrate[40], through the quantification of NADPH oxidation at 340 nm. Results are expressed in international units of enzyme activity (U). GR activity was performed using GSSG as substrate[40], through the spectrophotometric quantification of NADPH oxidation to $NADP^+$ at 340 nm. Results are expressed in international units of enzyme activity (U).

Superoxide Dismutase (SOD) activity was measured using a SOD activity kit purchased from Enzo Life Sciences (Farmingdale, New York). This is a colorimetric-based assay in which superoxide ions are generated in the presence of molecular oxygen from the conversion of xanthine to uric acid and hydrogen peroxide by the enzyme xanthine oxidase. The generated superoxide anions react with WST-1, converting it to WST-1 formazan, a colored product that absorbs light at 450 nm. When SOD is present, the amount of superoxide ion is reduced and consequently, the rate of WST-1 formazan formation decreases. The relative SOD activities of the hepatic tissue from control and obese ewes were expressed as a percentage of inhibition of the rate of WST-1 formazan formation. The assay was performed according to the kit manufacturer's instructions. Briefly, tissue samples were minced and rinsed three times in PBS to remove blood clots or other debris. The pelleted decanted fragments were resuspended in 1x extraction buffer supplied with the kit and homogenized for 20 seconds with an UltraTurrax homogenizer from IKA (Staufen, Germany) two times. The homogenates were kept on ice for 30 minutes and periodically vortexed. The disrupted tissue suspension was centrifuged at 10,000xg for 10 minutes at 4°C to remove insoluble material. The supernatants were recovered, maintained on ice, and protein concentration was determined by the BioRad-DC protein assay (Hercules, USA).

SOD activity determination was performed at 25°C using 200 µl of 1X SOD assay buffer supplemented with WST-1 reagent and xanthine oxidase. The reaction was initiated by adding xanthine solution and followed for 10 minutes through absorbance readings at 450 nm every minute using the Cytation 3 multi-mode microplate reader (BioTek Instruments, Inc.). Assays were performed in duplicates, and the results are expressed in enzyme units (U). A standard curve obtained with the purified SOD supplied with the kit was used to calculate enzyme activities. All the units are detailed in each plot.

Protein kinase A activity

Protein kinase A (PKA) activity was measured using the PKA kinase activity kit from Enzo Life Sciences (Farmingdale, New York). This assay is based on a solid-phase enzyme-

linked immuno-absorbent assay (ELISA). The multi-well plates provided in the kit are pre-coated with a synthetic peptide that is a specific substrate for PKA. Kinase activity is determined using a polyclonal antibody that specifically recognizes the phosphorylated form of the substrate.

Tissue homogenization was performed as described for the catalase activity assay, although a different extraction buffer was used (20 mM MOPS, 50 mM β-glycerophosphate, 50 mM sodium fluoride, 1 mM sodium orthovanadate, 5 mM EGTA, 2 mM EDTA, 1% NP40, 1 mM dithiothreitol (DTT), and 1mM phenylmethanesulfonylfluoride (PMSF)). Samples were left on ice for 10 minutes and centrifuged at 15 700 g for 15 minutes. The pellets were discarded, and the supernatants were used for PKA activity assessment after protein quantification. Briefly, samples (1 µg of protein) were added to each well, the reaction was started by the addition of ATP and allowed to occur for 90 minutes at 30°C. The wells were soaked with a solution of the phosphorylated substrate-specific antibody and incubated for 60 minutes at room temperature. The wells were washed during 1-2 minutes with the washing buffer provided in the kit a total of four times. Subsequently, the multi-well plates were incubated with a peroxidase-conjugated secondary antibody (anti-rabbit IgG: HRP conjugate) at room temperature for 30 minutes. Wells were rewashed four times as previously described. The assay was completed by adding the horseradish peroxidase substrate tetramethylbenzidine (TMB), leading to the generation of a colored product proportional to the PKA phosphotransferase activity. TMB reaction with the secondary antibody was followed at 650 nm for 45 minutes using Cytation 3. Then, the color development was stopped by adding an acidic stop solution, and the plates were re-read at 450 nm. PKA activity was assessed either using the slope from the kinetic record or the final absorbance since they provide similar results. PKA activity was normalized to the average of the control group.

NAD^+ and NADH levels

NAD^+ and NADH (oxidized and reduced nicotinamide adenine dinucleotides, respectively) levels and their ratio was measured using NAD/NADH-Glo™ Assay purchased

from Promega Corporation (Madison, Wyoming). This assay uses a NAD cycling enzyme that converts NAD+ to NADH in a specific substrate provided in the kit. NADH is used by the enzyme reductase to reduce a proluciferin reductase substrate to form luciferin. Luciferin is quantified using Ultra-Glo™ Recombinant Luciferase (rLuciferase), and the light signal produced was proportional to the amount of NAD^+ or NADH in the sample.

Samples were homogenized as described for the catalase assay but using a bicarbonate buffer (100 mM sodium carbonate, 20 mM sodium bicarbonate, 10 mM nicotinamide, 0.05% Triton X-100, pH 10) with 1% dodecyltrimethylammonium bromide (DTAB). Samples were centrifuged at 15 700 g for 15 minutes and the pellet was discarded. Each sample was split into two microtubes to measure NAD^+ with one and NADH with the other. In general, oxidized forms are selectively destroyed by heating in a basic solution, while reduced forms are not stable in acidic solutions. To measure NAD^+ levels, 50 µL of samples (0.4 mg of protein/mL) were incubated with 25 µL of 0.4 N HCL and heated at 60°C for 15 minutes. Samples were left for 10 minutes at room temperature before adding 25 µL of 0.5M Trizma base, pH 10.7. For NADH levels measurement, 50 µL of samples (0.4 mg of protein/mL) were heated at 60°C for 15 minutes. After cooling down the samples for 10 minutes at room temperature, 50 µL of 0.4 M HCl/ 0.5 M Trizma base was added. Then 20 µL of samples were mixed with 20 µL of the NAD/NADH-Glo™ detection reagent in a Corning 384-well low flange white flat bottom polystyrene not treated microplate. After 1 h incubation, luminescence was measured in a Cytation 3 multi-mode microplate reader (BioTek Instruments, Inc.). NAD^+ and NADH levels were normalized using the control group values, while their ratio was determined directly from the raw data.

Malondialdehyde (MDA), Reduced and Oxidized Glutathione (GSH and GSSG), and Vitamin E quantification

For GSH, GSSG, MDA, and Vitamin E quantifications, the samples' extraction protocol was as previously described for the GPx activity determination. Measurements of GSH and GSSG levels were performed as described previously[39]. The OxisResearch kit (Percipio

Biosciences Burlingame, CA, USA) was used according to the manufacturer's instructions. This assay is based on a method that follows absorbance changes at 420 nm due to the formation of a chromophoric thione that occurs proportionally to GSH concentration[41]. Results are expressed as μmol (μM) of GSH or GSSG per μg of protein. Lipid peroxidation was assessed by quantification of malondialdehyde (MDA) adducts separated by HPLC (Gilson, Lewis Center, Ohio, USA) using the ClinRep complete kit (Recipe, Munich, Germany) as described by the manufacturer. Fluorescence readings with emission at 553 nm and excitation at 515 nm were performed using a Jasco FP-2020/2025 fluorescence detector (Jasco, Tokyo, Japan). Vitamin E levels were quantified by reverse-phase high-performance liquid chromatography (HPLC) using an analytic column Spherisorb S10w (250 x 4.6mm). Elution was performed with 0.9% methanol in n-hexane at a flow of 1.5 mL/min. Vitamin E was quantified using absorbance reading at 287 nm and internal standards.

Mitochondrial Respiratory Chain (MRC) complexes and Citrate Synthase (CS) enzymatic activities

The samples were homogenized as described for the catalase assay, except that 50 mM phosphate buffer (pH 7.0) was used as a buffer. Citrate synthase activity was measured according to a previously described protocol[42]. The reaction was started by the addition of 30 μL of each sample (2 mg/mL) to the wells containing 80 μL of 1 mM 5,5'-Dithiobis(2-nitrobenzoic acid) (DTNB), 10 μL of 4 mM acetyl-CoA, 10 μL of 1% Triton X-100 (in 50 mM phosphate buffer pH 7.0) and 20 μL of 10 mM oxaloacetate. The reaction was followed by the absorbance increase at 412 nm due to the consumption of DTNB and the formation of 5-Mercapto-2-nitrobenzoic acid (TNB). The baseline activity was measured for 2 minutes and the increase of absorbance was followed for 5 minutes after starting the reaction. The assay was performed in triplicates. Negative controls were obtained by replacing oxaloacetate with 50 mM phosphate buffer (pH 7.0). Citrate synthase activity was determined using the slope of the experimental values' linear regression and was expressed in enzyme units (U) obtained by the

Beer-Lambert law with l=0.346 cm and Ɛ=13.6 $mmol^{-1}.cm^{-1}$. Citrate synthase activity of the negative controls was subtracted from their respective samples.

MRC Complex I (NADH dehydrogenase) activity was determined according to a previously described protocol[43]. To each reaction well was added 130 µL H_2O, 21 µL potassium phosphate buffer (PB) 500 mM pH 7.5, 12.6 µL BSA 50 mg/mL, 6 µL KCN 10 mM, 10 µL NADH 2 mM, and 10 µL of the sample to be tested with a 2 mg/mL protein concentration (20 µg total protein). The reaction was started by adding 6 µL decylubiquinone 10 mM and the decrease of absorbance at 340 nm due to oxidation of NADH was followed. The baseline activity was measured for 5 minutes before de addition of decylubiquinone. The decrease in absorbance was followed for 10 minutes after starting the reaction. To check the specificity of the reaction, 12.5 µM of the complex I inhibitor rotenone was added in separate wells. In the wells, without rotenone, the volume was adjusted with 50 mM PB pH 7.0. Each sample was measured in triplicates and negative controls were in duplicates. The maximal activity was determined using the slope of the experimental values' linear regression and is expressed in enzyme units (U) obtained by the Beer-Lambert law with l = 0.484 cm and Ɛ = 6.2 $mmol^{-1}.cm^{-1}$. NADH dehydrogenase activity of the negative controls was subtracted from their respective samples.

MRC Complex II (succinate dehydrogenase) activity was measured according to a previously described protocol[43]. An aliquot of 80 µL from the sample homogenate at 2 mg/mL protein was incubated with 12.5 µL PB 25 mM pH 7.5, 5 µL BSA 50 mg/mL, 145 µL DCPIP 0.015% and 7.5 µL KCN 10 mM. The reaction was started by adding 12.5 µL of the complex II substrate succinate (400 mM). Succinate dehydrogenase activity was followed by the decrease of absorbance at 600 nm due to DCPIP reduction. The baseline activity was measured for 2 minutes and the decrease in absorbance was followed for 3 minutes after starting the reaction. To check the specificity of the reaction, 10 µL of the complex II inhibitor malonate (1 M) was added in separate wells. Linear regression of the experimental values was used to obtain slopes. The slope from the baseline was subtracted from the slope from complex II

activity. The assay was performed in triplicates. Activities are presented in enzyme units (U) using the Beer-Lambert law with l = 0.628 cm and Ɛ = 19.1 $M^{-1}.cm^{-1}$.

Complex I/III activity was measured according to a previously described protocol[43]. An aliquot of 25 µL from the sample homogenate at 2 mg/mL protein concentration was incubated with 175 µL H_2O for 10 minutes. After, a mix containing 25 µL PB 50 mM pH 7.5, 5 µL BSA 50 mg/mL, 7.5 µL 10 mM KCN, and 2.5 µL NADH 10 mM was added to each well. The reaction was started by the addition of 12.5 µL of cytochrome c 1 mM and followed by the increase of absorbance at 550 nm due to the reduction of cytochrome c. The baseline activity was measured for 2 minutes and the decrease in absorbance was followed for 2 minutes after starting the reaction. To check the specificity of the reaction, negative controls obtained using 2.5 µL of both the complex I and III inhibitors, rotenone (1 mM) and antimycin A (10 $mg.mL^{-1}$), respectively, were performed in separate wells. Linear regression of the experimental values was used to obtain slopes. Complex I+III specific activity was obtained by subtracting the activity of negative controls from the activity of the respective sample. Activity is expressed in enzyme units using the Beer-Lambert law with l = 0.625 cm and Ɛ = 18.5 $M^{-1}.cm^{-1}$.

Complex II/III activity was measured according to a previously described protocol[43]. A mix containing 100 µL PB 25 mM pH 7.5, 7.5 µL KCN 10 mM, and 6.25 µL succinate 400 mM was added to 15 µL of sample homogenates with 2 mg/mL protein concentrations. The reaction was started by adding 12.5 µL of cytochrome c 1 mM and followed by the increase of absorbance at 550 nm due to the reduction of cytochrome c. The baseline activity was measured for 2 minutes, and the increase of absorbance was followed for 3 minutes after starting the reaction. To check the specificity of the reaction, 2.5 µL of complex II inhibitor, malonate (1 M), was added in separate wells. Sample activities were performed in duplicates, and the slope of the negative control was subtracted from the total slope. Linear regression of the experimental values was used to obtain slopes. Activity is expressed in enzyme units (U) using the Beer-Lambert law with l = 0.331 cm and Ɛ = 18.5 $M^{-1}.cm^{-1}$.

Complex IV (cytochrome c oxidase) activity was measured according to a previously described protocol[43]. The reaction was started by the addition of 12 µL of the complex IV

substrate, reduced cytochrome c 1 mM, to a mix containing 170 µL PB 50 mM pH 7.0 and 37.5 µL sample homogenates with a 2 mg/mL protein concentration. Cytochrome c was reduced using sodium dithionite according to a protocol previously described[43]. Briefly, oxidized cytochrome c was prepared in 20 mM PB pH 7.0. Cytochrome c was reduced, immediately before use, by mixing with a few grains of sodium dithionite in the tip of a pipette. The solution's color changed from brown to red-pink. Cytochrome c reduction was confirmed by measuring the ratio between absorbance values at 550 nm and 565 nm. A ratio greater than 6 indicates that cytochrome c was successfully reduced and that the solution is adequate to be used[43]. The MRC complex IV reaction was followed by the decrease of absorbance at 550 nm due to the oxidation of cytochrome c. The baseline activity was measured for 2 minutes and the decrease in absorbance was followed for 3 minutes after starting the reaction. To check the specificity of the reaction, 6 µL of the complex IV inhibitor KCN (10 mM) was added in separate wells. Linear regression of the experimental values was used to obtain slopes. All the assays were performed in duplicates, the activity is expressed in enzyme units (U) and was obtained using the Beer-Lambert law with $l = 0.519$ cm and $\varepsilon = 18.5\ M^{-1}.cm^{-1}$.

Immunoblotting

A piece of tissue with ~30 mg was homogenized two times for 20 seconds with an Ultra-Turrax homogenizer from IKA (Staufen, Germany) in RIPA buffer (50 mM Tris pH 8, 150 mM NaCl, 5 mM EDTA, 15 mM MgCl2, 1% TritonX-100) supplemented with 0.5 mM PMSF, 2.5‰ of a protease inhibitor cocktail (104 mM AEBSF, 80 µM Aprotinin, 4 mM Bestatin, 1.4 mM E-64, 2 mM Leupeptin, and 1.5 mM Pepstatin A), 20 mM NaF, 10 mM NAM, 5 mM Sodium Butyrate, 0.5% DOC and PhosSTOP (phosphatase inhibitor cocktail, Roche, Sigma -Aldrich Quimica) as described by the supplier. After homogenization, samples were centrifuged at 250 g for 2 minutes at 4°C, and the pellet was discarded. Protein was quantified, and the samples were diluted to 2.4 mg/mL with supplemented RIPA buffer. Laemmli buffer 6 times concentrated (375 mM Tris-HCl (pH 6.8), 9% SDS, 50% glycerol, 9% beta-mercaptoethanol, 0.03% bromophenol blue, and 300 mM DTT) was added to each sample to

achieve a final protein concentration of 2 mg/mL. Samples were boiled at 95°C for 5 minutes (except for an aliquot which was used in Oxidative phosphorylation system (OXPHOS) cocktail protein quantification). Samples were stored at -20°C until future use.

Samples (25 µg of protein) were loaded in 10% or 12% acrylamide gels. In each gel, Precision Plus Protein Dual Color Standards and a positive control consisting of 25 µg of protein from HepG2 extracts were run in parallel with the samples. Electrophoresis was performed at room temperature with running buffer (25 mM Tris, 192 mM glycine, 0.1% SDS), at constant current intensity (30 mA per gel) in a Mini-PROTEAN tetra Cell (Bio-Rad) for around 75 minutes. Protein was then transferred to PVDF membranes in a Trans-Blot Turbo Transfer System (Bio-Rad). PVDF membranes were activated by incubation for 1 minute in methanol, 5 minutes in ddH2O, and 15 minutes in Trans-Blot Turbo Transfer Buffer (Bio-Rad). Transference occurred for 10 minutes at constant current intensity (2.5 A). Transfer quality was assessed by ponceau staining the membranes.

According to the antibodies' datasheet, membranes were then blocked using 5% free-fat milk or 5% BSA, in TBS-T buffer (Tris 20 mM, pH 8.0, NaCl 150 mM, Tween-20 0.1% (w/v)) for 2 hours at room temperature. Membranes were washed 3 times with TBS-T, for at least 5 minutes each time and under agitation, and incubated with primary antibody (Table S5) overnight, under agitation at 4°C. Unless stated otherwise in the supplier documentation, primary antibodies were prepared in 1% free-fat milk in TBS-T buffer. Membranes were washed 3 times again as previously described and incubated with the secondary antibody (Table S6) prepared in TBS-T buffer, for 2 hours, at room temperature and under agitation.

After the incubation with the secondary antibody, membranes were washed 3 times as previously described, except that TBS (TBS-T without Tween-20) was used instead of TBS-T. Membranes were then incubated with Clarity Western ECL Substrate (Bio-Rad) for 5 minutes and images were collected with a UVP BioSpectrum 500 imaging System (UVP, Upland, California). Images were analyzed with the TotalLab TL120 software (Nonlinear Dynamics, Newcastle, UK), using the background subtraction method 'Rolling Ball' with radius = 50. The volume of the bands was used to compare protein expression between different lanes. ATP5a

results from the average quantification of two different protein epitopes. Results were normalized by β-actin expression or ponceau S staining and are reported relative to the control group's mean.

Data analysis and statistics

Two-sided statistical tests were always used. Data were analyzed using GraphPad Prism 8.0.2 (GraphPad Software, Irvine, CA. USA) and results are expressed as median, 1st quartile (Q_1), and the 3rd quartile (Q_3) with three significant digits. The number of experiments performed in each assay is represented in each plot.

To measure MO-related differences, comparisons were performed between Control (C) and Maternal Obesity (MO) values in liver lobes pool (C vs. MO) and each lobe, between Maternal liver (ML) Left Lobe-Control (MLL-C) and ML Left Lobe-MO (MLL-MO), and between ML Right Lobe-Control (MLR-C) and ML Right Lobe-MO (MLR-MO). Data points were excluded if identified as outliers by the ROUT method with Q=1%. The normality of the results' distribution was evaluated using the Shapiro-Wilk normality test (α=0.05). If the data presented a normal distribution, a parametric unpaired t-test was performed. Otherwise, the Mann–Whitney test was used. To compare liver lobes, comparisons between MLL-C and MLR-C, and MLL-MO and MLR-MO were performed using paired statistical tests. Wilcoxon test and parametric paired t-test were used according to data normality. Statistical test values with $p<0.05$ were considered statistically significant differences.

The comparison of responders vs. non-responders in the MO group was performed using a parametric unpaired t-test ($p < 0.10$ was considered statistically significant) and performed a Pearson correlation using the weight at the c-section ($R > 0.60$ or $R < -0.60$ were considered statistically significant).

For the computational data analysis, Python 3 version 3.7.3, and the Pandas and SciPy packages were used. Correlation matrices and cluster maps were plotted using Matplotlib and Seaborn modules. A correlation value of +1 indicated a total positive linear correlation, −1 a total negative correlation, and 0 identifies the inexistence of linear correlation. Cluster maps

were plotted to relate features (in columns) with instances (in rows), with the color of each cell representing the normalized level of expression of a particular feature in a specific instance. The information is grouped both in rows and columns by a two-way hierarchical clustering method using the squared Euclidean distance metric for both dendrograms. Missing values were interpolated to the average of the same condition.

Results

Maternal Obesity Morphometrics Outcomes

Maternal body weight was measured at three time-points: before the diet intervention, at conception, and before the cesarean section. Similar ewe weights were observed in C and MO groups at the start of obesogenic diet consumption (p=0.57). However, a significant difference existed at conception (after 60 days of diet intervention, C.vs.MO: median=69.0kg, Q_1=57.9, Q_3=84.0 vs. median= 78.5kg, Q_1=73.5, Q_3=94.5; p=0.05; Figure 1A). At 0.9G, MO weight was still increased (C.vs.MO: median=102kg, Q_1=91.3, Q_3=115 vs. median=111kg, Q_1=105, Q_3=121; p=0.05) and was accompanied by enlarged subcutaneous fat thickness (C.vs.MO: median=2.00 cm, Q_1=2.00, Q_3=2.12 vs. median=3.75 cm, Q_1=3.50, Q_3=4.50; p=0.003; Figure 1B).

No differences in the heart (p=0.90), liver (p=0.20), and brain (p=0.62) absolute weight were observed between the C and MO groups (Figure 1C).

Effects of Maternal Obesity During Pregnancy on Mitochondrial Biology

Liver disease and some PALD (i.e. HELLP syndrome and AFLD) are associated with mitochondrial structural and functional modulation resembling NAFLD progression-associated mitochondrial dysfunction[20,22,23]. We found no alteration in the master-regulator of mitochondrial biogenesis[44] PGC-1α (p=0.11, Figure S1A) protein amount in the hepatic tissue. However, hepatic PPARγ protein levels, coactivated by PGC-1α, were slightly decreased (C.vs.MO: median=0.985, Q_1=0.820, Q_3=1.23 vs. median=0.879, Q_1=0.635, Q_3=1.07; p=0.057; Figure S1C) in MO. Interestingly, both PPARγ and PGC-1α are more expressed in MLR than in MLL (Figure 2B) in control (PPAR γ: p<0.0001; PGC-1α: p=0.03) and MO (PPAR γ: p=0.003; PGC-1α: p=0.003) livers. MO-related PGC-1α and PPARγ hepatic alterations are also exclusive to MLR with lower PPAR γ (p=0.004) and higher PGC-1α (p=0.01) protein abundance.

To understand whether MO during gestation may trigger liver disease and induces alterations in MRC, protein expression of different MRC complexes and ATP synthase subunits

were assessed in a liver lobe pool and in the separated two main liver lobes. MO increased ATP synthase ATP5a subunit (C.vs.MO: median=0.971, Q_1=0.921, Q_3=1.07 vs. median=1.08, Q_1=0.961, Q_3=1.44; p=0.03; Figure 2C) while decreasing MRC subunits protein expression: complex-I subunit Ndufs8 (C.vs.MO: median=0.952, Q_1=0.808, Q_3=1.20 vs. median=0.882, Q_1=0.696, Q_3=0.988; p=0.066), complex-II subunits SDHA (C.vs.MO: median=0.841, Q_1=0.652, Q_3=1.13 vs. median=0.671, Q_1=0.588, Q_3=0.797; p=0.048) and SDHB (C.vs.MO: median=0.957, Q_1=0.640, Q_3=1.20 vs. median=0.304, Q_1=0.202, Q_3=0.575; p<0.01), complex-III subunit UQCRFS1 (C.vs.MO: median=0.887, Q_1=0.726, Q_3=1.28 vs. median=0.777, Q_1=0.542, Q_3=0.991; p=0.062), and complex-IV subunit mtCO1 (C.vs.MO: median=0.924, Q_1=0.778, Q_3=1.21 vs. median=0.672, Q_1=0.569, Q_3=0.867; p<0.01). Complex-III subunits UQCRC1 (p=0.13) and UQCRC2 (p=0.56), and complex-IV COX-II (p=0.19) protein abundance were not altered in MO (Figure 2C).

MO during pregnancy exhibited lobe-specific mitochondrial effects. While SDHB (MLL-C.vs.MLL-MO: p<0.01; MLR-C.vs.MLR-MO: p<0.01) and mtCO1 (MLL-C.vs.MLL-MO: p=0.010; MLR-C.vs.MLR-MO: p=0.064) protein expression was equally decreased in both MO-liver lobes, MO-related decrease in Ndufs8 (p=0.025) and UQCRFS1 (p=0.038) was more pronounced in the left lobe, while MO-decreased SDHA (p=0.018) and a slight, but not statistically significant, increase in ATP5a (p=0.087) were predominately observed in MLR (Figure 2E). MLL presents a lower variation of correlation between MRC subunits due to MO (Figure 2D, dashed), while more significant correlation differences are observed in MLR (Figure 2D, delimited). SDHA is implied in the top five losses of positive correlation in MO, four in the MLR, and one in the MLL (Figure 2D, red). Intriguingly, the correlation between the two complex-II subunits SDHA and SDHB is one of the most affected (Figure S1B). In opposition, in the top five of increased correlations in MO, two MRC subunits stand out: UQCRC1 with two correlations and the mtDNA-encoded mtCO1 involved in three (Figure 2D, blue; Figure S1B).

To assess if MO-induced alterations in protein expression translated into altered protein activity, we measured MRC maximal enzymatic activities. Complex-I activity was 53%

increased in MO (C.vs.MO: median=2.43, Q_1=1.84, Q_3=3.62 vs. median=3.99, Q_1=3.00, Q_3=5.59; p=0.005; Figure 3A) with similar increases observed in both lobes (MLL-C.vs.MLL-MO: p=0.073; MLR-C.vs.MLR-MO: p=0.014). The complex-II activity was decreased by 20% in MO (C.vs.MO: median=108, Q_1=94.1, Q_3=130 vs. median=87.1, Q_1=77.1, Q_3=97.7; p=0.0048) in both lobes (MLL-C.vs.MLL-MO: p=0.0234; MLR-C.vs.MLR-MO: p=0.03; Figure 3B). No alteration occurred in the combined activity of complex-I/complex-III and complex-II/complex-III in total hepatic tissue nor when comparing liver lobes. MO exhibited a 2-fold increase in complex-IV maximum activity (C.vs.MO: median=1.50, Q_1=0.981, Q_3=2.27 vs. median=2.62, Q_1=1.38, Q_3=5.07; p=0.02; Figure 3E) with a greater impact in MLR (p=0.04).

Despite the changes found in MRC complexes' activities and subunits' protein expression the conventional mitochondrial mass indicators determined remained unchanged: CS activity (p=0.46; Figure 3G), mtDNA copy number (p=0.69; Figure 3H), and mitochondria-related protein expression (CS: p=0.37; TOM20: p=0.20; Figure 4E). When we correlated MRC complex activity with the respective subunit protein expression, the top three MO-increased correlations were Ndufs8, COX-II, and the complex-II catalytic subunit SDHA, all in the MLL (Figure 3F, delimited; Figure S1D). In contrast, SDHB expression and activity positive correlation was lost in MLL-MO. Interestingly, none of the top differences were identified in MLR, suggesting another level of activity regulation rather than protein expression, e.g. supercomplexes assembly or post-translational modifications.

Hepatic Metabolic Regulation in Obesity During Pregnancy

To clarify the maternal hepatic adaptations in MO vs. C pregnancies, we assessed PKA activity and the redox state (Figure 4). PKA activity is regulated by cyclic adenosine monophosphate levels obtained from ATP decomposition, thus is dependent on ATP concentration and production. PKA activation regulates several cell functions through phosphorylation, including cell differentiation, growth, development, and metabolism affecting

mitochondrial dynamics, hepatic lipid accumulation, and MRC complexes activity, including complex-IV inhibition[45,46].

Despite the unaltered PKA protein abundance (p=0.38; Figure 4E), PKA kinase activity was 40% decreased in MO total liver tissue (C.vs.MO: median=0.945, Q_1=0.775, Q_3=1.33 vs. median=0.477, Q_1=0.347, Q_3=0.832; p=0.0007; Figure 4A). MO livers had decreased ANT isoforms 1/2 (C.vs.MO: median=0.996, Q_1=0.757, Q_3=1.17 vs. median=0.693, Q_1=0.567, Q_3=0.891; p=0.0035; Figure 4E) and VDAC (C.vs.MO: median=0.945, Q_1=0.763, Q_3=1.18 vs. median=0.708, Q_1=0.633, Q_3=0.956; p=0.012; Figure 4E) protein expression, advocating that ATP transport through mitochondrial membranes may be impaired, leading to lower PKA activity.

The hepatic redox state was also indirectly assessed by the NAD^+/NADH ratio, being 35.8% increased in MO (C.vs.MO: median=0.640, Q_1=0.595, Q_3=0.657 vs. median=0.775, Q_1=0.674, Q_3=1.07; p=0.0059; Figure 4D) due to a 19.9% reduction of NADH levels (C.vs.MO: median=0.977, Q_1=0.960, Q_3=1.07 vs. median=0.850, Q_1=0.769, Q_3=0.926; p=0.0004; Figure 4C), rather than by alterations in NAD^+ levels (p=0.80; Figure 4B).

The MO-associated alterations during pregnancy were lobe-dependent with greater impact in MLR (Figure 4; Figure S2): PKA kinase activity decrease was more pronounced in MLR (MLR-C.vs.MLR-MO: median=0.975, Q_1=0.858, Q_3=1.29 vs. median=0.434, Q_1=0.328, Q_3=0.530; p<0.0001) as well as NADH reduced levels (MLR-C.vs.MLR-MO: median=1.02, Q_1=0.954, Q_3=1.08 vs. median=0.806, Q_1=0.522, Q_3=0.870; p=0.0070), and consequent NAD^+/NADH ratio increase (MLR-C.vs.MLR-MO: median=0.605, Q_1=0.508, Q_3=0.629 vs. median=0.987, Q_1=0.719, Q_3=1.10 p<0.01; Figure 4D). Even though ANT 1/2 protein expression was decreased in both liver lobes, it was only statistically significant in MLR (C.vs.MO: MLR–p=0.019, MLL–p=0.096; Figure S2A). The VDAC protein expression was equally decreased in the liver lobes (C.vs.MO: MLR–p=0.025, MLL–p=0.043; Figure S2A) being expressed differently between lobes in MO (MLR-MO.vs.MLL-MO, p=0.0024). Lobe-dependent protein expression in control samples (MLR-C.vs.MLL-C) was also observed for CS (p=0.0008), TOM20 (p=0.039), and VDAC (p=0.0039; Figure S2A).

Obesity in Pregnancy Effects on Hepatic Oxidative Stress

Despite reduced MRC subunits protein expression, obesity-related excessive nutrition, and complex-I and complex-IV increased activities can lead to increased reactive oxygen species (ROS) production and oxidative stress state. MDA, a by-product of lipid peroxidation was increased by 48% in MO livers (C.vs.MO: median=8.22, Q_1=6.73, Q_3=9.53 vs. median=12.1, Q_1=9.23, Q_3=14.2; $p<0.01$; Figure 5A), being the difference consistent between liver lobes (C.vs.MO: MLR-p=0.045, MLL-p=0.016). Although no alterations in vitamin E levels (p=0.81; Figure 5B) were found, MO hepatic tissue presented a decrease in GSH/GSSG ratio (C.vs.MO: median=6.01, Q_1=4.80, Q_3=8.36 vs. median=3.37, Q_1=2.32, Q_3=4.69; p=0.0052; Figure 5E). The decreased ratio was mainly caused by increased GSSG levels found in MO livers (median=9.41, Q_1=5.73, Q_3=12.97 vs. median=14.4, Q_1=11.3, Q_3=23.9; p=0.011; Figure 5D) without variation in GSH levels (p=0.28; Figure 5C). A contrasting liver lobe-selective behavior is observed in the GSH levels in MO: values were elevated in MLL (p=0.044) and reduced in MLR (p=0.030).

Oxidized glutathione accumulation may be a consequence of a high oxidative environment, an impairment in the enzymatic glutathione system, or both[47]. GR protein expression (C.vs.MO: median=0.894, Q_1=0.754, Q_3=1.22 vs. median=0.739, Q_1=0.585, Q_3=0.918; p=0.034; Figure 6E) and activity (C.vs.MO: median=100, Q_1=86.8, Q_3=119 vs. median=75.6, Q_1=70.9, Q_3=88.9; p=0.067; Figure 6D), as well as Gpx-4 protein expression (C.vs.MO: median=0.942, Q_1=0.698, Q_3=1.21 vs. median=0.805, Q_1=0.166, Q_3=1.01; p=0.024; Figure 6E), and Gpx activity (C.vs.MO: median=105, Q_1=90.3, Q_3=133 vs. median=89.0, Q_1=75.9, Q_3=110; p=0.084; Figure 6C) were decreased in MO livers, despite increased protein levels for Gpx-1 (C.vs.MO: median=1.00, Q_1=0.846, Q_3=1.08 vs. median=1.17, Q_1=0.986, Q_3=1.55; p=0.014; Figure 6E). Alterations in glutathione-related proteins were larger in MLR. Here, decreased Gpx-4 protein levels (p=0.019), and GR activity (p=0.021) and protein levels (p=0.0031) were observed compared to MLR-C. In fact, decreased GR (p=0.064) and Gpx-4 (p=0.0048) protein expression were already observed in MLR compared with MLL in control

samples. Although not statistically significant, the same trend was observed in MO livers for Gpx-4 (p=0.074), while increased GR (p=0.078) was detected in MLR compared with MLL.

MO livers revealed increased total SOD activity (C.vs.MO: median=0.650, Q_1=0.310, Q_3=0.874 vs. median=0.908, Q_1=0.631, Q_3=1.06; p=0.035; Figure 6A), predominantly in MLR (MLR-C.vs.MLR-MO, p=0.083). Catalase activity (C.vs.MO: median=1708, Q_1=1457, Q_3=1973 vs. median=1458, Q_1=875, Q_3=1755; p=0.028; Figure 6B) and protein expression (C.vs.MO: median=1.02, Q_1=0.898, Q_3=1.08 vs. median=0.876, Q_1=0.588, Q_3=1.08; p=0.031; Figure 6E) were decreased in MO-liver. The decrease in catalase activity in MO was more extensive in MLL (MLL-C.vs.MLL-MO, p=0.043) while decreased protein expression was more significant in MLR (MLR-C.vs.MLL-MO, p=0.015).

Integrative Data Analysis

To deeper comprehend the hepatic impact of obesity during pregnancy on maternal mitochondrial function and oxidative stress, we plotted the correlation between the assessed parameters in C (Figure 7A) and MO (Figure 7B). Considerable alterations in the correlation profile between both groups exist, which are characteristic of metabolic and redox different hepatic adaptations to pregnancy during MO (Figure 7C).

We performed a Principal Component Analysis (PCA) with all samples, obtaining a perfect separation between C and MO hepatic samples (Figure S3A). Remarkably, there is also a significant separation of samples based on the liver lobe. Similar results were obtained when the dataset was restricted to six samples per group to minimize missing values imputation. By using the parameters evaluated in this work, the samples naturally clustered according to the respective group (i.e., C and MO) in an almost perfect way (Figure 7D). Based on this clustering, we also obtained a notable separation according to the liver lobe, suggesting a liver lobe-dependent metabolic and redox remodeling in both MO and control samples. The condition-dependent separation (i.e., MLR-C, MLL-C, MLR-MO, and MLL-MO) was confirmed in the PCA of the restricted dataset (Figure 8A).

To understand which parameters were most relevant for separating the samples by condition (C.vs.MO) during pregnancy, we first identified the features that better discriminate between C and MO samples in each liver lobe independently, based on the difference between groups and the p-value observed in the volcano plot (Figure 8B). The most relevant parameters were PKA activity in MLR, SDHB protein expression in both lobes, GR protein expression in MLR, and NAD^+/NADH ratio. When comparing C and MO hepatic samples, these parameters were in the top eight features with more significant information gain (Figure S3B). Surprisingly, four of the five most discriminative parameters are from the MLR. When the comparison between liver lobes was plotted, the highlighted features were VDAC protein expression in C and MO, Gpx-4 protein expression in C, and SDHB protein expression and GSH levels in MO (Figure 8C).

We observed that different parameters are responsible for the spatial distribution of samples according to the PCA (Figure S3C). Specific features are responsible for clustering the samples in the respective groups in this PCA (Figure 8D). Interestingly, some of the parameters that separate the samples according to the group are lobe-dependent (Figure 8E). Thus, we selected the top five parameters that presented the highest information gain based on the discrimination between conditions (Figure 8F). By restricting the dataset to these features (SDHB, VDAC, and ANT1/2 protein expression, NADH levels, and NAD^+/NADH ratio), we obtained a perfect clustering of the samples by C vs. MO as well as for each liver lobe independently (Figure 8G). The PCA corroborates this observation (Figure 8H), suggesting a distinctive metabolic remodeling in both liver lobes during pregnancy that is present in control samples and retained in MO. We evaluated the clustering of the samples in the PCA using a logistic regression algorithm (Figure S3D) which correctly predicted the condition of 23 out of 24 samples, being the unique mismatch wrongly attributed to the MO group of the respective MLL group (Figure S3E).

We also evaluated the potential bimodal pattern of weight gain and the possibility of the existence of responders and non-responders in the MO group based on the weight at c-section. Then we perform a direct comparison between the two groups using very relaxed statistical

thresholds to evaluate whether the potential bimodal pattern on weight gain has indeed a molecular and cellular correspondence on the hepatic tissue(Figure S4A-B). We also performed a simple Pearson correlation coefficient using soft thresholds. Only four features in the right liver lobe, one feature in the left liver lobe, and one morphological feature showed any relation with the differential behavior of weight gain in obese pregnant sheep (Figure S4 C-H). There is no common feature associated with weight at the c-section between lobes. Importantly, all the correlations are lost when adding the control individuals.

Discussion

MO during pregnancy represents a major metabolic burden for the organism due to both the combination of obesity-metabolic impairment and physiological pregnancy-demanding adaptations. Previous epidemiological studies associated MO with increased maternal disease development (e.g. diabetes, cardiovascular disease) throughout and after gestation, including liver disease [3,6]. However, cellular and molecular mechanisms underlying this association are poorly characterized. To the best of our knowledge, this is the first report identifying the maternal-specific hepatic metabolic adaptations that are characteristic of an obese pregnancy and describing the mitochondrial implications in a lobe-dependent fashion.

We studied a well-characterized ewe overfeeding MO model, which induces total body weight and body fat percentage increase[35]. The present cohort presented a similar increase in total body weight at conception and c-section and increased subcutaneous fat thickness, the predominant place of fat accumulation[48]. The no alterations in liver weight during MO pregnancy are a potential result of pregnancy-induced hepatomegaly, observed in normative gestations in humans[49] and rodents[50,51], which attenuates the hepatic MO-related increase in liver size to 14% at 0.9G. Increased Alanine Aminotransferase (ALT) and Alkaline Phosphatase activities were reported in this model with a greater impact on ALT activity in the right liver lobe, suggesting higher hepatic damage in MO during pregnancy[13].

MO-Associated Hepatic Oxidative Stress During Gestation

Systemic oxidative stress is common during a healthy pregnancy resulting from a normal pregnancy-related inflammatory response[7,21]. Several factors impact maternal liver function during gestation: the placental-related ROS production, the rise in circulating toxic molecules from fetal origin, the pregnancy-associated metabolic and energetic requirements, among others[2,6,7]. Hepatic oxidative stress plays a crucial role in HELLP syndrome pathophysiology[6,23]. MO itself is a major risk factor for liver disease during pregnancy, probably due to hepatic obesity-exacerbated oxidative stress prior to pregnancy[8].

The MRC is one of the significant contributors to ROS generation under stress and pathological conditions, mainly at complex-I and complex-III, where superoxide anion is formed[52]. Since complex-I activity was increased in obese MLR, ROS production by complex-I is a plausible contributor to the increased oxidative damage[53]. Accordingly, increased SOD activity, the enzyme responsible for superoxide anion degradation and H_2O_2 production, was observed in MO livers, more evident in MLR.

Two enzymatic systems are responsible for further H_2O_2 degradation: catalase and the glutathione system[52]. Lower catalase expression and activity were observed in MO livers at late-gestation. Furthermore, we also found differences in the glutathione system due to MO. Gpx activity was decreased in MO livers, consistent with lower Gpx-4 protein expression. The results suggest a compromised hepatic H_2O_2 degradation system in MO at term gestation. Consequently, homeostatic dysregulation towards oxidative stress is expected.

Oxidative stress-derived protein modifications, such as in exposed cysteines and methionines, can lead to post-translational protein modifications impacting the protein's activity, solubility, and stability[54]. Interestingly, hepatic Gpx-1 protein expression is increased in MO, contrasting with Gpx enzymatic activity, which might result from Gpx activity inhibition due to modifications caused by high concentrations of H_2O_2[55]. Potential increased H_2O_2 concentrations stimulate hydroxyl radical formation through the Fenton reaction[52]. Increased lipid peroxidation and GSSG levels were observed in MO livers at term gestation, likely due to increased hydroxyl radical formation[56]. Lower GR protein expression and enzymatic activity can explain glutathione modulation by compromising cell ability to restore GSH levels[47]. Concomitantly, GSH/GSSG ratios are decreased due to GSSG accumulation and reduced GSH due to the overall oxidant environment resulting from obesity during gestation in MLL. The GSH levels decrease, and unchanged GSSG in MLR may result from a compromised glutathione synthesis.

An increased NAD^+/NADH ratio due to reduced NADH levels was observed in MO, exclusively in MLR at late gestation. NAD^+/NADH ratio and NADH levels are two of the five more relevant features of integrative data analysis to distinguish between control and MO

samples and liver lobes. NADH deprivation is associated with elevated nutrient consumption, increased oxidative phosphorylation and regulation of fatty acid metabolism[57]. The GSH/GSSG decreased ratio suggests that obesity during pregnancy is associated with ML-redox state alterations, which potentially can give rise to liver pathologies including NAFLD[58].

MO-Linked Hepatic Mitochondrial Modulation at Term Gestation

Gestation-related metabolic and energetic demands modulate maternal metabolism to fulfill pregnancy demands, including at the hepatic level[2]. Additionally, overnutrition propels the liver to shift metabolic pathways by increasing anabolism to manage the excessive availability of nutrients[59]. When prolonged in time, newly formed lipids accumulate in hepatocytes, a phenotype typical of NAFLD. We observed lower PPARγ and unaltered protein levels of its coactivator PGC-1α which have been related to the progression of liver fibrosis and increased collagen production[60]. The maternal hepatic metabolic switch due to MO during pregnancy may involve hepatic PI3K/AKT signaling pathway leading to mTORC1 signaling disruption at late-gestation (0.76G and 0.9G)[12,14] and switching hepatic fatty acid profile[16,17], impacting on PI3K/AKT crosstalk with PKA.

Protein Kinase A is one of the metabolic master-regulator kinases. This kinase is responsible for the phosphorylation of several enzymes that modulate hepatic metabolism, and its inhibition is associated with accelerated hepatic lipid accumulation[45,46,61]. Lower PKA activity was measured in the liver of MO ewes during gestation, exclusively in MLR. PKA activity also affects mitochondrial function, regulating MRC activity, mitochondrial dynamics, and apoptosis, through phosphorylation of multiple protein-sites, including DRP inhibition, Bad suppression, Bim stabilization, and Bax activation[45]. Several studies have shown that PKA can be translocated to the mitochondrial matrix and phosphorylate numerous PKA substrates inside mitochondria, including complex-I and complex-IV subunits. PKA inhibition decreased protein levels of complex-I subunits NDUFA9, NDUFV2, and NDUFS4, which are rescued by adding 8-Br-cAMP, a PKA substrate[62]. Similarly, complex-IV subunits I, IV1, and Vb

phosphorylation by PKA induces their degradation and the consequent decrease in complex-IV activity, putatively by compromising complex-IV stability[63].

Decreased protein expression of complex-I subunit Ndufs8, complex-II subunits SDHA and SDHB, complex-III subunit UQCRFS1, and complex-IV subunit mtCO1 were measured in MO livers at term-pregnancy. Indeed, in the present study, the reduction in complex-I Ndufs8 subunit protein levels and the increased complex-IV activity, possibly resulting from lower protein degradation in MO hepatic tissue at term pregnancy, might be a consequence of the observed decrease in PKA activity. On the other hand, this general decrease in MRC complexes subunits protein expression might potentially result from ROS-related damage accumulation, verified by increased lipid peroxidation, affecting proteins' stability, and targeting them to degradation[64]. Interestingly, mtDNA-encoded MRC subunits mtCO1 and COX-II protein expression correlated better in MO rather than C in MLR. Both proteins are associated with five of the top ten most altered correlations in MO hepatic tissue at late-gestation. The complex-II catalytic subunit SDHA registered the most significant loss of correlation with the other subunits assessed in this work due to MO. SDHB decreased protein expression represents one of the most relevant features in the integrative data analysis that separates the control and MO hepatic samples at term pregnancy according to the respective condition. Interestingly, only the complex-III UQCRFS1 subunit is slightly decreased in MO livers; however, UQCRFS1 is critical for complex-III maturation and proper function[65].

Potential mechanisms responsible for the general decrease in MRC subunits expression include mtDNA damage and/or the impairment of the mitochondrial protein import mechanisms. This scenario would lead to the synthesis of dysfunctional MRC proteins and/or compromised import of OXPHOS proteins into mitochondria[66,67]. The mtDNA damage can lead to stoichiometric imbalances between mtDNA- and nuclear-encoded OXPHOS subunits, potentially jeopardizing the complexes' assembly and decreasing protein levels[67].

The observation of lower hepatic complex-II activity in MO agrees with the decreased expression of the complex-II subunits SDHA and SDHB. In opposition, increased complex-I and complex-IV activities were observed, contrasting with decreased protein expression in late-

pregnancy MO. The observed unaltered activities of combined complexes I+III and II+III are most likely the result of a saturated quinone pool, which compromises complex-III ideal stimulation, or a reduced complex-III enzymatic activity compared with complexes-I or -II. In fact, complex-I and complex-II present, by themselves, different impacts on complex-III activity[68].

Alterations in MRC protein expression and activities are a well-established mechanism by which the hepatic redox state is altered, explaining the increased NAD^+/NADH ratio in MLR. We hypothesize that excessive nutrient uptake stimulates hepatocytes to increase their catabolic rate, accelerating Krebs' cycle turnover. As a result, more NADH and succinate are produced, stimulating the OXPHOS, and promoting ATP production. Increased Krebs' cycle turnover unsynchronized with OXPHOS can enhance ROS generation, impairing OXPHOS and emphasizing the dysfunction of this process[69].

Variations in mitochondrial number/mass could explain the differences in OXPHOS subunits expression and complexes' activities. However, no mitochondrial number differences nor mitochondrial biogenesis were observed between the experimental groups, as assessed by mtDNA copy number, CS activity, and TOM20 and PGC-1α protein expression levels, respectively. The apparent contradiction in the results might also be caused by the effects on the assembly and/or stability of supercomplexes formed by complex-I and complex-IV in MO livers at 0.9G. A higher mitochondrial efficiency would explain increased enzymatic activity concomitant with lower protein expression due to the formation of supercomplexes. Indeed, the formation of supercomplexes containing complex-I, III, and/or IV, but not complex-II, and their physical association with enzymes involved in mitochondrial fatty acid β-oxidation have been observed in the liver[70], supporting the reported increase in fatty acid oxidation in late-pregnancy[7]. It has also been proposed that these molecular associations may modulate the subtle energy metabolism dysfunction, characteristic of pathologies with increased cellular fatty acids levels, such as obesity and type 2 diabetes[70]. This mechanism, however, fails to explain the absence of alterations in complexes-I+III activity, considering complexes subunits' expression and activities observed in this work.

The apparent lower protein abundance of VDAC and ANT 1/2 in MO livers at late-gestation, independent of the unaltered mitochondrial mass markers, suggests that the mitochondria might have a compromised ability to transport metabolites and ions across the outer mitochondrial membrane. Decreased hepatic ANT may prevent hepatic steatosis and insulin resistance since ANT depletion is protective against these conditions[71]. Additionally, these are two parameters with higher information gain in the integrative data analysis to distinguish the samples between conditions.

Maternal Hepatic Lobe-Dependent Effects of Obesity During Pregnancy

This work shows that the adaptations to maternal obesity during pregnancy in the right and left liver lobes are distinct. This conclusion is supported by sample clustering analysis, which clearly distinguished C and MO samples and achieved a significant clustering based on the liver lobe. Accordingly, PCA resulted in the good separation of the samples related to their physiological condition and liver lobe (e.g., MLR-C, MLR-MO, MLL-C, and MLL-MO). This separation becomes almost perfect in a PCA of the dataset with the top five informative parameters. Moreover, the clustering analysis of the restricted dataset perfectly clustered the samples according to the condition. This integrative data analysis supports the observations that, although a common effect of MO during pregnancy at 0.9G exists in both hepatic liver lobes, some mechanisms are lobe-dependent.

In an obese and pregnant organism, MLR undergoes further metabolic adaptations compared with MLL, namely in PKA activity, redox state (e.g., NAD+/NADH), and decreased enzymatic antioxidant capacity (SOD and GR activities; catalase, Gpx-4, and GR protein levels). The higher protein levels of PPARγ and the co-activator PGC-1α observed in MLR in comparison to MLL might explain the increased flexibility of the right liver lobe to coupe with the MO stimuli during gestation and modulate downstream pathways, such as MRC subunits and antioxidant defense protein expression. It has been described that decreasing PPARγ protein levels via PGC-1α or NRF-2 modulation ameliorated mitochondrial function and hepatic steatosis[72,73].

Conclusions

The emphasis on the consequences of maternal obesity during pregnancy has been on fetal programming changes. We have provided important data that assess the maternal impact. Identifying the maternal metabolic adaptations in MO is critical to understand the milieu to which fetuses were exposed during development and the long-term consequences on the offspring's health. Here we describe the exclusive hepatic effects of obesity during pregnancy at late-gestation, without discriminating the potential contribution of pregnancy per se or the pre-pregnancy obesity implications. This is the limitation of this work since we cannot evaluate whether just pregnancy itself can contribute to hepatic disease exacerbation. Despite the described protective role of pregnancy for other diseases, such as breast and endometrial cancers.

We show here for the first time that obesity during pregnancy results in altered maternal hepatic mitochondrial function and redox state at late-gestation, which potentially predisposes to hepatic dysfunction during and after pregnancy (Figure 9).

In the present work, we found a common MO impact in both hepatic lobes. Obesity during gestation induced an increase in complex-I and complex-IV activities, possibly caused by β-oxidation stimulation[70], leading to ROS overproduction and molecular damage, as observed by lipid peroxidation, decreasing OXPHOS subunits expression. At term gestation, a more extensive MO-impact on MLR is observed compared to MLL. Obesity during pregnancy can be an early-event predisposing for maternal hepatic pathophysiology and NAFLD development. Moreover, the modulation of the maternal endocrine-metabolic axis will have a critical impact on fetal development and offspring predisposition to metabolic disease[74].

If extended to other hepatic pathologies, this lobe dichotomy can be critical in liver disease diagnosis, biopsies analysis, and liver transplantation. Monitoring liver function during the challenging pregnancy period can provide new insights to understand hepatopathology and prevent complications in both the mother and offspring throughout and after gestation.

Conflict-of-interest/financial disclosure statement

The authors declare that they have no conflict of interest or relationship with industry. The funding agencies had no role in study design, data collection and analysis, decision to publish, or preparation of this document.

Data availability statement

The data that support the findings of this study are openly available in Figshare [75].

Author contributions

LG- Methodology, Investigation, Writing the original draft, Data curation, Formal analysis, Visualization

CHC, CT, IB, JDM, MD, TO – Methodology, Investigation, Review, and Editing final version

PWN, SF - Conceptualization, Funding acquisition, Project administration, Resources, Writing, Review, and Editing

PO - Funding acquisition, Project administration, Resources, Writing, Review

SP - Conceptualization, Data curation, Project administration, Resources, Supervision, Writing, Review, and Editing the final version

References

[1] Stang J, Huffman LG. Position of the Academy of Nutrition and Dietetics: Obesity, Reproduction, and Pregnancy Outcomes. J Acad Nutr Diet 2016;116:677–91. https://doi.org/10.1016/j.jand.2016.01.008.

[2] Gilmore LA, Klempel-donchenko M, Redman LM. Pregnancy as a window to future health : Excessive gestational weight gain and obesity. Semin Perinatol 2015:1–8. https://doi.org/10.1053/j.semperi.2015.05.009.

[3] Kriebs JM. Obesity in Pregnancy - Addressing Risks to Improve Outcomes 2014;28:32–40. https://doi.org/10.1097/JPN.0000000000000008.

[4] Godfrey KM, Reynolds RM, Prescott SL, Nyirenda M, Jaddoe VWV, Eriksson JG, et al. Influence of maternal obesity on the long-term health of offspring. Lancet Diabetes Endocrinol 2017;5:53–64. https://doi.org/10.1016/S2213-8587(16)30107-3.

[5] Farpour-Lambert NJ, Ells LJ, Martinez de Tejada B, Scott C. Obesity and Weight Gain in Pregnancy and Postpartum: an Evidence Review of Lifestyle Interventions to Inform Maternal and Child Health Policies. Front Endocrinol (Lausanne) 2018;9:546. https://doi.org/10.3389/FENDO.2018.00546.

[6] Westbrook RH, Dusheiko G, Williamson C. Pregnancy and liver disease. J Hepatol 2016;64:933–45. https://doi.org/10.1016/j.jhep.2015.11.030.

[7] Mouzon SH, Lassance L. Endocrine and metabolic adaptations to pregnancy ; impact of obesity 2015;24:65–72. https://doi.org/10.1515/hmbci-2015-0042.

[8] Lisonkova S, Razaz N, Sabr Y, Muraca GM, Boutin A, Mayer C, et al. Maternal risk factors and adverse birth outcomes associated with HELLP syndrome: a population-based study. BJOG An Int J Obstet Gynaecol 2020. https://doi.org/10.1111/1471-0528.16225.

[9] Jiang R, Wang T, Li B, He J. Clinical characteristics and pregnancy outcomes of atypical hemolysis, elevated liver enzymes, and low platelets syndrome: A case series. Medicine (Baltimore) 2020;99:e19798. https://doi.org/10.1097/MD.0000000000019798.

[10] Wu K, Yin B, Li S, Zhu X, Zhu B. Prevalence, risk factors and adverse perinatal outcomes for Chinese women with intrahepatic cholestasis of pregnancy: a large cross-sectional retrospective study. Ann Med 2022;54:2966–74. https://doi.org/10.1080/07853890.2022.2136400.

[11] Valdovinos-Bello V, García-Romero CS, Cervantes-Peredo A, García-Gómez E, Martínez-Ibarra A, Vázquez-Martínez ER, et al. Body mass index implications in intrahepatic cholestasis of pregnancy and placental histopathological alterations. Ann Hepatol 2023;28. https://doi.org/10.1016/J.AOHEP.2022.100879.

[12] Musial B, Fernandez-Twinn DS, Duque-Guimaraes D, Carr SK, Fowden AL, Ozanne SE, et al. Exercise alters the molecular pathways of insulin signaling and lipid handling in maternal tissues of obese pregnant mice 2019;7. https://doi.org/10.14814/phy2.14202.

[13] Grilo L, Viegas I, Diniz M, Tocantins C, Martins J, Ford S, et al. Maternal obesity (MO) during pregnancy induces maternal liver damage and compromises fetal hepatic function. Eur. J. Clin. Investig. Vol. 51, 111 RIVER ST, HOBOKEN 07030-5774, NJ USA: Wiley; 2021, p. 22–3.

[14] Musial B, Vaughan OR, Fernandez-Twinn DS, Voshol P, Ozanne SE, Fowden AL, et al. A Western-style obesogenic diet alters maternal metabolic physiology with consequences for fetal nutrient acquisition in mice. J Physiol 2017;595:14. https://doi.org/10.1113/JP273684.

[15] Bowman CE, Alpergin ESS, Cavagnini K, Smith DM, Scafidi S, Wolfgang MJ. Maternal Lipid Metabolism Directs Fetal Liver Programming following Nutrient Stress Correspondence. Cell Rep 2019;29. https://doi.org/10.1016/j.celrep.2019.09.053.

[16] Muir R, Liu G, Khan R, Shmygol A, Quenby S, Gibson RA, et al. Maternal obesity-induced decreases in plasma, hepatic and uterine polyunsaturated fatty acids during labour is reversed through improved nutrition at conception OPEN. Sci REpoRtS | 2018;8:3389. https://doi.org/10.1038/s41598-018-21809-9.

[17] Stevanović-Silva J, Beleza J, Coxito P, Pereira S, Rocha H, Gaspar TB, et al. Maternal high-fat high-sucrose diet and gestational exercise modulate hepatic fat accumulation and liver mitochondrial respiratory capacity in mothers and male offspring. Metabolism 2021;116:154704. https://doi.org/10.1016/j.metabol.2021.154704.
[18] Svegliati-Baroni G, Pierantonelli I, Torquato P, Marinelli R, Ferreri C, Chatgilialoglu C, et al. Lipidomic biomarkers and mechanisms of lipotoxicity in non-alcoholic fatty liver disease. Free Radic Biol Med 2019;144:293–309. https://doi.org/10.1016/j.freeradbiomed.2019.05.029.
[19] Samuel VT, Shulman GI. Nonalcoholic Fatty Liver Disease as a Nexus of Metabolic and Hepatic Diseases. Cell Metab 2018;27:22–41. https://doi.org/10.1016/j.cmet.2017.08.002.
[20] Simões ICM, Fontes A, Pinton P, Zischka H, Wieckowski MR. Mitochondria in non-alcoholic fatty liver disease. Int J Biochem Cell Biol 2018;95:93–9. https://doi.org/10.1016/j.biocel.2017.12.019.
[21] Chiarello DI, Abad C, Rojas D, Toledo F, Vázquez CM, Mate A, et al. Oxidative stress: Normal pregnancy versus preeclampsia. Biochim Biophys Acta - Mol Basis Dis 2020;1866. https://doi.org/10.1016/j.bbadis.2018.12.005.
[22] Natarajan SK, Thangaraj KR, Goel a., Eapen CE, Balasubramanian K a., Ramachandran a. Acute fatty liver of pregnancy: an update on mechanisms. Obstet Med 2011;4:99–103. https://doi.org/10.1258/om.2011.100071.
[23] Bu S, Wang Y, Sun S, Zheng Y, Jin Z, Zhi J. Role and mechanism of AT1-AA in the pathogenesis of HELLP syndrome. Sci Rep 2018;8:1–9. https://doi.org/10.1038/s41598-017-18553-x.
[24] Hui SCN, So H kwan, Chan DFY, Wong SKH, Yeung DKW, Ng EKW, et al. Validation of water-fat MRI and proton MRS in assessment of hepatic fat and the heterogeneous distribution of hepatic fat and iron in subjects with non-alcoholic fatty liver disease. Eur J Radiol 2018;107:7–13. https://doi.org/10.1016/j.ejrad.2018.08.008.
[25] Friedrich-Rust M, Romen D, Vermehren J, Kriener S, Sadet D, Herrmann E, et al. Acoustic radiation force impulse-imaging and transient elastography for non-invasive assessment of liver fibrosis and steatosis in NAFLD. Eur J Radiol 2012;81:e325–31. https://doi.org/10.1016/j.ejrad.2011.10.029.
[26] Bonekamp S, Tang A, Mashhood A, Wolfson T, Changchien C, Middleton MS, et al. Spatial distribution of MRI-determined hepatic proton density fat fraction in adults with nonalcoholic fatty liver disease. J Magn Reson Imaging 2014;39:1525–32. https://doi.org/10.1002/jmri.24321.
[27] Jacobsson H, Jonas E, Hellström PM, Larsson SA. Different concentrations of various radiopharmaceuticals in the two main liver lobes: A preliminary study in clinical patients. J Gastroenterol 2005;40:733–8. https://doi.org/10.1007/s00535-005-1617-9.
[28] Nilsson H, Karlgren S, Blomqvist L, Jonas E. The inhomogeneous distribution of liver function: Possible impact on the prediction of post-operative remnant liver function. Hpb 2015;17:272–7. https://doi.org/10.1111/hpb.12348.
[29] Gebhardt R, Matz-Soja M. Liver zonation: Novel aspects of its regulation and its impact on homeostasis. World J Gastroenterol 2014;20:8491–504. https://doi.org/10.3748/wjg.v20.i26.8491.
[30] Kessler J, Rasmussen S, Kiserud T. The fetal portal vein: normal blood flow development during the second half of human pregnancy. Ultrasound Obstet Gynecol 2007;30:52–60. https://doi.org/10.1002/uog.4054.
[31] Cox LA, Schlabritz-Loutsevitch N, Hubbard GB, Nijland MJ, McDonald TJ, Nathanielsz PW. Gene expression profile differences in left and right liver lobes from mid-gestation fetal baboons: a cautionary tale. J Physiol 2006;572:59–66. https://doi.org/10.1113/jphysiol.2006.105726.
[32] Hocher B, Haumann H, Rahnenführer J, Reichetzeder C, Kalk P, Pfab T, et al. Maternal eNOS deficiency determines a fatty liver phenotype of the offspring in a sex dependent manner. Epigenetics 2016;11:539–52. https://doi.org/10.1080/15592294.2016.1184800.
[33] Su Y-M, Lv G-R, Xie J-X, Wang Z-H, Lin H-T. Maternal Hypoxia Increases the

Susceptibility of Adult Rat Male Offspring to High-Fat Diet-Induced Nonalcoholic Fatty Liver Disease. Endocrinology 2013;154:4377–87. https://doi.org/10.1210/en.2012-1683.
[34] Grilo LF, Tocantins C, Diniz MS, Gomes RM, Oliveira PJ, Matafome P, et al. Metabolic Disease Programming: From Mitochondria to Epigenetics, Glucocorticoid Signalling and Beyond. Eur J Clin Invest 2021. https://doi.org/10.1111/eci.13625.
[35] George LA, Uthlaut AB, Long NM, Zhang L, Ma Y, Smith DT, et al. Different levels of overnutrition and weight gain during pregnancy have differential effects on fetal growth and organ development. Reprod Biol Endocrinol 2010;8:75. https://doi.org/10.1186/1477-7827-8-75.
[36] Tuersunjiang N, Odhiambo JF, Long NM, Shasa DR, Nathanielsz PW, Ford SP. Diet reduction to requirements in obese/overfed ewes from early gestation prevents glucose/insulin dysregulation and returns fetal adiposity and organ development to control levels. Am J Physiol Endocrinol Metab 2013;305. https://doi.org/10.1152/AJPENDO.00117.2013.
[37] Council NR. Nutrient Requirements of Small Ruminants. Washington, D.C.: National Academies Press; 2007. https://doi.org/10.17226/11654.
[38] Grilo LF, Martins JD, Cavallaro CH, Nathanielsz PW, Oliveira PJ, Pereira SP. Development of a 96-well based assay for kinetic determination of catalase enzymatic-activity in biological samples. Toxicol Vitr 2020;69. https://doi.org/10.1016/j.tiv.2020.104996.
[39] Freitas M, Baldeiras I, Proença T, Alves V, Mota-Pinto A, Sarmento-Ribeiro A. Oxidative stress adaptation in aggressive prostate cancer may be counteracted by the reduction of glutathione reductase. FEBS Open Bio 2012;2:119–28. https://doi.org/10.1016/j.fob.2012.05.001.
[40] Horn H-D. Methods of enzymatic analysis. 2011.
[41] Tsao S-M, Yin M-C, Liu W-H. Oxidant Stress and B Vitamins Status in Patients With Non-Small Cell Lung Cancer. Nutr Cancer 2007;59:8–13. https://doi.org/10.1080/01635580701365043.
[42] Quirós PM. Determination of Aconitase Activity: A Substrate of the Mitochondrial Lon Protease. Methods Mol. Biol., vol. 1731, 2018, p. 49–56. https://doi.org/10.1007/978-1-4939-7595-2_5.
[43] Spinazzi M, Casarin A, Pertegato V, Salviati L, Angelini C. Assessment of mitochondrial respiratory chain enzymatic activities on tissues and cultured cells. Nat Protoc 2012;7:1235–46. https://doi.org/10.1038/nprot.2012.058.
[44] Wan X, Zhu X, Wang H, Feng Y, Zhou W, Liu P, et al. PGC1α protects against hepatic steatosis and insulin resistance via enhancing IL10-mediated anti-inflammatory response. FASEB J 2020;34:10751–61. https://doi.org/10.1096/FJ.201902476R.
[45] Ould Amer Y, Hebert-Chatelain E. Mitochondrial cAMP-PKA signaling: What do we really know? Biochim Biophys Acta - Bioenerg 2018;1859:868–77. https://doi.org/10.1016/j.bbabio.2018.04.005.
[46] Yang J, Zhang X, Yi L, Yang L, Wang WE, Zeng C, et al. Hepatic PKA inhibition accelerates the lipid accumulation in liver. Nutr Metab 2019;16:69. https://doi.org/10.1186/s12986-019-0400-5.
[47] Li L, Zhang G-F, Lee K, Lopez R, Previs SF, Willard B, et al. A Western diet induced NAFLD in LDLR−− mice is associated with reduced hepatic glutathione synthesis. Free Radic Biol Med 2016;96:13–21. https://doi.org/10.1016/j.freeradbiomed.2016.03.032.
[48] Goossens GH. The Metabolic Phenotype in Obesity: Fat Mass, Body Fat Distribution, and Adipose Tissue Function. Obes Facts 2017;10:207–15. https://doi.org/10.1159/000471488.
[49] Bartlett AQ, Vesco KK, Purnell JQ, Francisco M, Goddard E, Guan X, et al. Pregnancy and weaning regulate human maternal liver size and function. Proc Natl Acad Sci U S A 2021;118:2107269118. https://doi.org/10.1073/PNAS.2107269118/-/DCSUPPLEMENTAL.
[50] Bustamante JJ, Copple BL, Soares MJ, Dai G. Gene profiling of maternal hepatic adaptations to pregnancy. Liver Int 2010;30:406–15. https://doi.org/10.1111/J.1478-

3231.2009.02183.X.
[51] Milona A, Owen BM, Van Mil S, Dormann D, Mataki C, Boudjelal M, et al. The normal mechanisms of pregnancy-induced liver growth are not maintained in mice lacking the bile acid sensor Fxr. Am J Physiol Gastrointest Liver Physiol 2010;298. https://doi.org/10.1152/AJPGI.00336.2009.
[52] Sies H. Hydrogen peroxide as a central redox signaling molecule in physiological oxidative stress: Oxidative eustress. Redox Biol 2017;11:613–9. https://doi.org/10.1016/j.redox.2016.12.035.
[53] Bournat JC, Brown CW. Mitochondrial dysfunction in obesity. Curr Opin Endocrinol Diabetes Obes 2010;17:446–52. https://doi.org/10.1097/MED.0b013e32833c3026.
[54] Dahl JU, Gray MJ, Jakob U. Protein quality control under oxidative stress conditions. J Mol Biol 2015;427:1549–63. https://doi.org/10.1016/j.jmb.2015.02.014.
[55] Cho C-S, Lee S, Lee GT, Woo HA, Choi E-J, Rhee SG. Irreversible Inactivation of Glutathione Peroxidase 1 and Reversible Inactivation of Peroxiredoxin II by H_2O_2 in Red Blood Cells. Antioxid Redox Signal 2010;12:1235–46. https://doi.org/10.1089/ars.2009.2701.
[56] Jarukamjorn K, Jearapong N, Pimson C, Chatuphonprasert W. A High-Fat, High-Fructose Diet Induces Antioxidant Imbalance and Increases the Risk and Progression of Nonalcoholic Fatty Liver Disease in Mice. Scientifica (Cairo) 2016;2016:1–10. https://doi.org/10.1155/2016/5029414.
[57] Xie N, Zhang L, Gao W, Huang C, Huber PE, Zhou X, et al. NAD+ metabolism: pathophysiologic mechanisms and therapeutic potential. Signal Transduct Target Ther 2020;5:1–37. https://doi.org/10.1038/s41392-020-00311-7.
[58] Serviddio G, Bellanti F, Vendemiale G. Free radical biology for medicine: learning from nonalcoholic fatty liver disease. Free Radic Biol Med 2013;65:952–68. https://doi.org/10.1016/J.FREERADBIOMED.2013.08.174.
[59] Koo S-H. Nonalcoholic fatty liver disease: molecular mechanisms for the hepatic steatosis. Clin Mol Hepatol 2013;19:210. https://doi.org/10.3350/cmh.2013.19.3.210.
[60] Francque S, Szabo G, Abdelmalek MF, Byrne CD, Cusi K, Dufour JF, et al. Nonalcoholic steatohepatitis: the role of peroxisome proliferator-activated receptors. Nat Rev Gastroenterol Hepatol 2021;18:24–39. https://doi.org/10.1038/S41575-020-00366-5.
[61] Lu M, Shyy JY-J. Sterol regulatory element-binding protein 1 is negatively modulated by PKA phosphorylation. Am J Physiol Physiol 2006;290:C1477–86. https://doi.org/10.1152/ajpcell.00374.2005.
[62] De Rasmo D, Signorile A, Santeramo A, Larizza M, Lattanzio P, Capitanio G, et al. Intramitochondrial adenylyl cyclase controls the turnover of nuclear-encoded subunits and activity of mammalian complex I of the respiratory chain. Biochim Biophys Acta - Mol Cell Res 2015;1853:183–91. https://doi.org/10.1016/j.bbamcr.2014.10.016.
[63] Prabu SK, Anandatheerthavarada HK, Raza H, Srinivasan S, Spear JF, Avadhani NG. Protein Kinase A-mediated Phosphorylation Modulates Cytochrome *c* Oxidase Function and Augments Hypoxia and Myocardial Ischemia-related Injury. J Biol Chem 2006;281:2061–70. https://doi.org/10.1074/jbc.M507741200.
[64] Stiburek L, Cesnekova J, Kostkova O, Fornuskova D, Vinsova K, Wenchich L, et al. YME1L controls the accumulation of respiratory chain subunits and is required for apoptotic resistance, cristae morphogenesis, and cell proliferation. Mol Biol Cell 2012;23:1010–23. https://doi.org/10.1091/mbc.E11-08-0674.
[65] Bottani E, Cerutti R, Harbour ME, Ravaglia S, Dogan SA, Giordano C, et al. TTC19 Plays a Husbandry Role on UQCRFS1 Turnover in the Biogenesis of Mitochondrial Respiratory Complex III. Mol Cell 2017;67:96-105.e4. https://doi.org/10.1016/j.molcel.2017.06.001.
[66] Harbauer AB, Zahedi RP, Sickmann A, Pfanner N, Meisinger C. The Protein Import Machinery of Mitochondria—A Regulatory Hub in Metabolism, Stress, and Disease. Cell Metab 2014;19:357–72. https://doi.org/10.1016/j.cmet.2014.01.010.
[67] Houtkooper RH, Mouchiroud L, Ryu D, Moullan N, Katsyuba E, Knott G, et al.

Mitonuclear protein imbalance as a conserved longevity mechanism. Nature 2013;497:451–7. https://doi.org/10.1038/nature12188.
[68] Genova ML, Bianchi C, Lenaz G. Supercomplex organization of the mitochondrial respiratory chain and the role of the Coenzyme Q pool: Pathophysiological implications. BioFactors 2005;25:5–20. https://doi.org/10.1002/biof.5520250103.
[69] Paradies G, Paradies V, Ruggiero FM, Petrosillo G. Oxidative stress, cardiolipin and mitochondrial dysfunction in nonalcoholic fatty liver disease. World J Gastroenterol 2014;20:14205–18. https://doi.org/10.3748/wjg.v20.i39.14205.
[70] Wang Y, Mohsen A-W, Mihalik SJ, Goetzman ES, Vockley J. Evidence for physical association of mitochondrial fatty acid oxidation and oxidative phosphorylation complexes. J Biol Chem 2010;285:29834–41. https://doi.org/10.1074/jbc.M110.139493.
[71] Cho J, Zhang Y, Park SY, Joseph AM, Han C, Park HJ, et al. Mitochondrial ATP transporter depletion protects mice against liver steatosis and insulin resistance. Nat Commun 2017;8. https://doi.org/10.1038/ncomms14477.
[72] Li L, Fu J, Liu D, Sun J, Hou Y, Chen C, et al. Hepatocyte-specific Nrf2 deficiency mitigates high-fat diet-induced hepatic steatosis: Involvement of reduced PPARγ expression. Redox Biol 2020;30. https://doi.org/10.1016/J.REDOX.2019.101412.
[73] Afonso MB, Islam T, Magusto J, Amorim R, Lenoir V, Simões R, et al. RIPK3 dampens mitochondrial bioenergetics and lipid droplet dynamics in metabolic liver disease. Hepatology 2022. https://doi.org/10.1002/HEP.32756.
[74] Grilo LF, Diniz MS, Tocantins C, Areia AL, Pereira SP. The endocrine-metabolic axis regulation in offspring exposed to maternal obesity – cause or consequence in metabolic disease programming? Obesities 2022;ISSN 2673-.
[75] Dataset https://figshare.com/articles/dataset/MNE_results_xlsx/19407197.

Figures Legends

Figure 1- Maternal morphological parameters from the control group (C) and maternal obesity group (MO). A: live weight before initiating the diet, conception, and c-section. B: subcutaneous fat thickness. C: maternal heart, liver, and brain weight at the c-section. The number of individuals in each group is indicated by the symbols in the plot.

Statistical analysis: Comparison between control and maternal obesity groups was performed using unpaired t-test in A (after performing Shapiro-Wilk normality test). P-value lower than 0.05 was considered significant (* $p \leq 0.05$; *** $p \leq 0.001$; **** $p \leq 0.0001$). Blue violin plot, C; Red violin plot, MO. Median, interquartile distance, minimum and maximum are depicted. Circles represent that the mother was pregnant with male fetuses and triangles with female fetuses.

Figure 2 – Impact of obesity during pregnancy (Maternal Obesity, MO) in hepatic metabolic transcription regulators and oxidative phosphorylation system (OXPHOS) complexes subunit levels. **A:** Experimental design applied in this study. **B:** Liver Lobe-dependent protein expression of PPARγ and PGC-1α. **C:** Alterations induced by MO in OXPHOS complexes subunits protein expression from the total hepatic tissue of C and MO: Complex-I (Ndufs8), Complex-II (SDHA, SDHB), Complex-III (UQCRC1, UQCRC2, UQCRFS1), Complex-IV (mtCO1, COX-II), and ATP Synthase (ATP5a). **D:** Difference of the correlation between complexes subunits protein expression in C and MO in each lobe. Circles show the nuclear (blue) or mitochondrial (orange) encoded origin of each subunit. Delimited rectangles highlight the top ten correlations with the largest difference between correlations in C and MO in each lobe. Dashed rectangles depict the ten correlations with a lower variation.
E: OXPHOS complexes subunits expression in the left and right liver lobes from C and MO. Protein squares expression was obtained by Western blot, showed in the heat map on the left (lower expression – blue, higher expression – red, average expression – white). The respective boxplot is represented on the right (Control – blue, MO – red). The statistics in black represent

the comparison between C and MO in the same liver lobe, in blue the comparison between both lobes of control samples, and in red between both lobes of MO. Missing values were replaced by the group's average in the heatmap but not considered for the boxplot and statistics. Data were normalized using the reference protein β-actin, while the protein expression was represented relative to the mean of the C group.

Statistical analysis: Comparison between C and MO groups was performed using the unpaired t-test except for the groups that did not pass the Shapiro-Wilk normality test (C: SDHA, UQCRC1, UQCRC2; MO: SDHB; MLL-C: SDHA, UQCRC2; MLL-MO: SDHB, mtCO1) in which the Mann-Whitney test was performed. Comparison between liver lobes was assessed using paired t-test or Wilcoxon test according to the normality of the groups compared. P-values lower than 0.10 were registered (# $p \leq 0.10$) and lower than 0.05 were considered significant (* $p \leq 0.05$; ** $p \leq 0.01$; *** $p \leq 0.001$; **** $p \leq 0.0001$). Blue violin plot, C; Red violin plot, MO. Median, interquartile distance, minimum and maximum are depicted. Circles represent that the mother was pregnant with male fetuses and triangles female fetuses.

Figure 3 – Modulation of hepatic enzymatic activities of Mitochondrial Respiratory Chain (MRC) complexes and mitochondrial mass markers by Maternal Obesity (MO) during pregnancy. MRC complexes activities were determined in total hepatic tissue from Control (C) and MO group or considering the contribution of each liver lobe: **A**: Complex-I, **B**: Complex-II, **C**: Complex-I+III, **D**: Complex-II+III, and **E**: Complex-IV activities. Data is represented in Units normalized per mass of protein used in each assay and by the mitochondrial mass marker citrate synthase activity. **F**: Difference of correlations between C and MO of complexes subunits protein expression and enzymatic activity complexes. Surrounded squares represent the five most significant differences between C and MO. Dashed lines highlight the correlations with a lower difference. Mitochondrial mass indicators' modulation due to MO was measured by **G:** Citrate synthase activity and **H:** mtDNA copy number. The number of individuals in each group is indicated by the number of symbols (circles represent mothers with male fetuses and triangles represent mothers with female fetuses).

Statistical analysis: Comparison between C and MO groups was performed using unpaired t-test in B, C, and D (after performing the Shapiro-Wilk normality test) and Mann-Whitney test in A and E. Comparison between lobes was assessed using paired t-test or Wilcoxon test according to the normality of the groups compared. P-values lower than 0.05 were considered significant (* $p \leq 0.05$; ** $p \leq 0.01$). Blue violin plot, C; Red violin plot, MO. Median, interquartile distance, minimum and maximum are depicted.

Figure 4 – Adaptation of the hepatic metabolic profile linked to Maternal Obesity (MO) during pregnancy compared to Control (C). **A:** Protein Kinase A activity; **B:** NAD^+ levels; **C:** NADH levels; **D:** NAD^+/NADH ratio and **E:** Protein expression of metabolism-related proteins ANT 1/2, citrate synthase, PKA, TOM20, and VDAC. Data is represented relative to the respective C group mean in A, B, C, and E. Data from Western blot was normalized using the reference protein β-actin. The number of individuals in each group is indicated by the number of symbols (circles represent mothers with male fetuses and triangles with female fetuses).

Statistical analysis: Comparison between C and MO groups was performed using unpaired t-test in A, B, D, and E (ANT 1/2 and PKA), after performing the Shapiro-Wilk normality test, and Mann-Whitney test in C and E (CS, TOM20 and VDAC). Comparison between lobes was assessed using paired t-test. P-values lower than 0.05 were considered significant (* $p \leq 0.05$, ** $p \leq 0.01$; *** $p \leq 0.001$; **** $p \leq 0.0001$). Blue violin plot, C; Red violin plot, MO. Median, interquartile distance, minimum and maximum are depicted.

Figure 5 - Maternal obesity (MO) during pregnancy increased hepatic oxidative stress measured by **A:** lipid peroxidation levels, **B:** vitamin E and **E:** GSH/GSSG ratio obtained from **C:** GSH, and **D:** GSSG levels. Data is represented in absolute concentrations normalized for the protein concentration. The number of individuals in each group is indicated by the number of symbols (circles represent mothers with male fetuses and triangles with female fetuses).

Statistical analysis: comparison between Control (C) and MO groups was performed using the unpaired t-test after passing the Shapiro-Wilk normality test in **A, B,** and **C** and using

the Mann-Whitney test in **D** and **E**. Comparison between lobes was assessed using unpaired t-test or Wilcoxon test according to the normality of the results. P-values lower than 0.10 were registered and lower than 0.05 were considered significant (* $p \leq 0.05$; ** $p \leq 0.01$). Blue violin plot, C; Red violin plot, MO. Median, interquartile distance, minimum and maximum are depicted.

Figure 6 – Hepatic antioxidant enzymatic defense modulation in Maternal Obesity (MO) during pregnancy. Alterations in the enzymatic antioxidant defense **A:** SOD; **B:** Catalase, **C:** Glutathione Peroxidase, and **D:** Glutathione Reductase activities. Protein expression variation of catalase, Gpx-1, Gpx-4, and GR **E:** in total liver tissue from C and MO groups, and **F:** the contribution of each lobe. Sample expression was obtained by Western blot, showed in the heat map on the left (lower expression – blue, higher expression – red, average expression – white). The respective boxplot is represented on the right (Control – blue, MO – red). The statistics in black represent the comparison between C and MO in the same liver lobe, in blue the comparison between both lobes of control samples, and in red between both lobes of MO. Missing values were replaced by the group's average in the heatmap, but not considered for the boxplot and statistical analyses. Data was normalized using the reference protein β-actin and the protein expression represented relative to the C group mean. The enzymatic activities are represented in Units normalized per protein mass used in each assay. The number of individuals in each group is indicated by the number of symbols (circles represent mothers with male fetuses and triangles with female fetuses).

Statistical analysis: Comparison between C and MO groups was performed using unpaired t-test, after passing Shapiro-Wilk normality test, except for Gpx and GR activities in which the Mann-Whitney test was used. Comparison between lobes was assessed using the Wilcoxon test except for Gpx-4 protein expression and enzymatic activities in which the paired t-test was performed. P-values lower than 0.10 (# $p \leq 0.10$) were registered and lower than 0.05 were considered significant (* $p \leq 0.05$; ** $p \leq 0.01$). Blue violin plot, C; Red violin plot, MO. Median, interquartile distance, minimum and maximum are depicted.

Figure 7 – Relation between the parameters measured to characterize the implications of obesity during pregnancy in the maternal liver at late-gestation. Correlation between each pair of analyzed parameters in **A:** control and **B:** Maternal obesity samples, and **C:** the respective difference between correlations. A correlation value of +1 (red) indicates a total positive linear correlation, −1 (blue) a total negative correlation, and 0 (white) identifies the inexistence of linear correlation. **D:** Heatmap showing the clustering of the samples and the parameters. Each parameter was normalized for the scale 0 to 1 (highest value in red and lower value in blue) and is named using the feature analyzed followed by the type of the assay (P stands for protein quantification, A for activity, Q for quantification, and R for the ratio).

Figure 8 – Analysis of the most relevant parameters to cluster the Control (C) and Maternal obesity (MO) samples. **A:** PCA of the dataset restricted to 24 samples (MLL-C – blue, MLL-MO – red, MLR-C – green, MLR-MO – orange). Volcano plots scoring the most relevant features in the **B:** comparison of C and MO samples in each liver lobe individually, and **C:** comparison between the liver lobes of each animal. In the PCA, **D:** some parameters are critical to distinguish between C and MO samples, and **E:** some of the features can also split the dataset according to the liver lobe of the samples. **F:** Information gain of each parameter to distinguish between the condition of the samples. **G:** Samples clustering according to a dataset restricted to the five most relevant parameters. Each parameter was normalized for the scale 0 to 1 (highest value in red and lower value in blue). **H:** PCA of the same restricted dataset showing a clear separation between the condition of the samples. Each parameter is named using the feature analyzed followed by the type of the assay (P stands for protein quantification, A for activity, Q for quantification, and R for the ratio).

Figure 9 – Schematic representation of the results obtained in this experimental study. Maternal obesity (MO) during pregnancy affects the oxidative phosphorylation system (OXPHOS)by modulating proteins' expression and enzymatic activities, leading to alterations in mitochondrial

metabolism and redox state. Obesity during pregnancy is associated with increased oxidative stress markers related to oxidative damage and impaired antioxidant enzymatic activity in a lobe-dependent manner.

Supplementary Material

Maternal hepatic adaptations during obese pregnancy encompass lobe-specific mitochondrial alterations and oxidative stress

Luís F. Grilo (1,2), luis.grilo@uc.pt

João D. Martins (1), jdgmartins@gmail.com

Mariana S. Diniz (1), marianasdiniz.diniz@gmail.com

Carolina Tocantins (1), carolina.tocantins.23.3@gmail.com

Chiara H. Cavallaro (1), chi.cavallaro@gmail.com

Inês Baldeiras (3), ines.baldeiras@sapo.pt

Teresa Cunha-Oliveira (1), teresa.oliveira@gmail.com

Stephen Ford (4), SPFord@uwyo.edu

Peter W. Nathanielsz (4), peter.nathanielsz@uwyo.edu

Paulo J. Oliveira (1), pauloliv@cnc.uc.pt

Susana P. Pereira (1,5), pereirasusan@gmail.com

1- CNC - Center for Neuroscience and Cell Biology, CIBB - Centre for Innovative Biomedicine and Biotechnology, University of Coimbra, UC-Biotech, Biocant Park, Cantanhede, Portugal

2 - Ph.D. Programme in Experimental Biology and Biomedicine (PDBEB), Institute for Interdisciplinary Research (IIIUC), University of Coimbra, Coimbra, Portugal

3-Neurological Clinic, Faculty of Medicine, University of Coimbra, Coimbra, Portugal

4 - Department of Animal Science, University of Wyoming, Laramie, WY, USA

5 - Laboratory of Metabolism and Exercise (LametEx), Research Centre in Physical Activity, Health and Leisure (CIAFEL), Laboratory for Integrative and Translational Research in Population Health (ITR), Faculty of Sport, University of Porto, Porto, Portugal

Keywords: gestation; maternal malnutrition; overnutrition; liver disease; hepatic mitochondria

Corresponding author: Susana P. Pereira, PhD

CNC-Center for Neuroscience and Cell Biology, UC Biotech, Biocant Park, University of Coimbra, 3060-197 Cantanhede, PORTUGAL

phone: +351-231-249-170,

fax: +351-239-853-409,

email: pereirasusan@gmail.com

ORCID: 0000-0002-1168-2444

Supplementary tables and figure legends

Table S1 - List of the reagents used in the present work, respective supplier, and commercial references.

Table S2 - Composition of the diet fed to ewes throughout the study.

Table S3 - Nutrient analysis of the experimental diet.

Table S4 - Sequences of the primers used for the quantification of mtDNA copy number.

Table S5 - List of primary antibodies used to perform protein determination by Western blot. 'Accession number' represents the UniProt (The Universal Protein Resource; https://www.uniprot.org/) reference of the protein and 'dilution' corresponds to the dilution used for each antibody during incubation.

Table S6 - List of secondary antibodies used in Western blot. 'Dilution' corresponds to the dilution used for each antibody during incubation.

Figure S1 - Protein expression of transcription regulators of hepatic metabolism and correlations of hepatic mitochondrial respiratory chain subunits protein expression and enzymatic activity in Control (C) and Maternal obesity (MO) groups. **A:** Protein expression of PPAR γ. **B:** Correlation between complexes subunits protein expression in C and MO in each lobe. Circles show the nuclear (blue) or mitochondrial (orange) encoded origin of each subunit. Bordered correlations highlight the top ten correlations with the largest difference between correlations in C and MO of the respective lobe. Dashed rectangles depict the ten correlations with the lowest variation. **C:** Protein expression of PGC-1α. **D:** Correlation between complexes subunits protein expression and the complexes' enzymatic activity. Surrounded rectangles

represent the five most significant differences between C and MO. Dashed lines highlight the correlations with the lowest difference. A correlation value of +1 indicated a total positive linear correlation, −1 a total negative correlation, and 0 identifies the inexistence of linear correlation.

Statistical analysis: Comparison between C and MO groups was performed using the unpaired t-test. P-values lower than 0.10 were registered. Blue violin plot, C; Red violin plot, MO. Median, interquartile distance, minimum and maximum are depicted. Circles represent that the mother was pregnant with male fetuses and triangles female fetuses.

Figure S2 - Hepatic metabolic-related protein expression modulation by maternal obesity during pregnancy. **A:** Protein levels of ANT 1/2, Citrate Synthase, Protein Kinase A, TOM 20, and VDAC in each lobe in Control (C) and Maternal Obesity (MO). Protein expression was obtained by Western blot, shown in the heat map on the left (lower expression – blue, higher expression – red, unaltered expression – white). The respective boxplot is represented on the right (Control – blue, MO – red). The statistics in black represent the comparison between C and MO in the same liver lobe, in blue the comparison between both lobes of control samples, and in red between both lobes of MO. The group's average replaced missing values in the heatmap but was not considered for the boxplot and statistics.

Statistical analysis: Comparison between control and MO groups was performed using unpaired t-test, after passing Shapiro-Wilk normality test, except for the comparison in the left lobe of VDAC protein expression in which the Mann Whitney test was used. Comparison between lobes was assessed using the Wilcoxon test except for VDAC (in MO) and CS (in control) protein expression, in which the unpaired t-test was performed. P-values lower than 0.10 were registered (#) and lower than 0.05 were considered significant (* $p \leq 0.05$; ** $p \leq 0.01$; *** $p \leq 0.001$).

Figure S3 - Distribution of the results according to integrative data analysis. **A:** PCA of all measured parameters and samples. Control samples (blue) and Maternal Obesity (MO) samples (red) present a great separation. Each number represents the animal, circles are used for the left liver lobe samples and crosses for the right liver lobe samples. **B:** Information gain

obtained for each parameter based on the comparison C vs. MO. **C:** Parameters weight in each component of the PCA for the dataset restricted to 24 samples. **D:** Evaluation of the sample's distribution based on the PCA restricted to 24 samples and the five most informative parameters through a logistic regression algorithm. **E:** Confusion matrix with the comparison of the predicted and the observed results of the distribution of samples according to the condition, based on the logistic regression algorithm. Each parameter is named using the feature analyzed followed by the type of the assay (P stands for protein quantification, A for activity, Q for quantification, and R for ratio).

Figure S4 – Bimodal pattern of weight at c-section in the Maternal Obesity (MO) group. **A:** Comparison of responders and non-responders in the MO group based on the p-value of unpaired t-test and Pearson correlation with weight at the c-section for the left liver lobe, **B:** and for the right liver lobe. Correlation between weight at the c-section and the significant parameters: **C:** Heart weight, **D:** VDAC, **E:** MDA, **F:** TOM20, **G:** NAD^+ / NADH, and **H:** Ndufs8.

Table S1 - List of the reagents used in the present work, respective supplier, and commercial references.

Reagent	CAS number	Supplier	Reference
Acetyl-CoA	102029-73-2	Sigma-Aldrich	A2056
Antimycin A	1397-94-0	Sigma-Aldrich	A8674
BioRad – DC protein assay	-	Bio-Rad	5000116
Bioxytech MD kit	-	OxisResearch	21044
Bromophenol blue	34725-61-6	Sigma-Aldrich	B5525
BSA (Bovine Serum Albumin)	9048-46-8	Sigma-Aldrich	A7030
Catalase from bovine liver	9001-05-2	Sigma-Aldrich	C1345
Clarity Western ECL substrate	-	Bio-Rad	1705060
Cytochrome C from bovine heart	9007-43-6	Sigma-Aldrich	30398
DCPIP (2,6-Dichloroindophenol sodium salt)	620-45-1	VWR	230212X
Decylubiquinone	55486-00-5	Sigma-Aldrich	D7911
Dimethyl malonate	108-59-8	Sigma-Aldrich	136441
DMSO (Dimethyl sulfoxide)	67-68-5	Sigma-Aldrich	34869
DNase/RNase-free water	-	Qiagen	1017979
DTAB (Dodecyltrimethylammonium bromide)	1119-94-4	Thermo Fisher	128271000
DTNB (5,5'-Dithiobis(2-nitrobenzoic acid)	69-78-3	Sigma-Aldrich	D8130
DTT (DL-1,4-Dithiothreitol)	3483-12-3	Sigma-Aldrich	D9779
EDTA (Ethylenediaminetetraacetic acid disodium salt)	6381-92-6	VWR	20296.291
EGTA (Ethylene-bis(oxyethylenenitrilo)tetraacetic acid)	67-42-5	Sigma-Aldrich	E4378
Glycerol	56-81-5	Sigma-Aldrich	G6279
Glycine	56-40-6	NZY tech	MB01401
GSSG (L-Glutathione oxidized)	27025-41-8	Sigma-Aldrich	G4376
HCl (Hydrochloric acid)	7647-01-0	Panreac	131020,1212
Hydrogen Peroxide	7722-84-1	Merck	107210
Isopropanol	67-63-0	Sigma-Aldrich	190764
K_2HPO_4 (Monobasic potassium phosphate)	7778-77-0	Sigma-Aldrich	NIST200B
KCl (Potassium chloride)	7447-40-7	Sigma-Aldrich	P9541
KCN (Potassium cyanide)	151-50-8	Fisher Scientific	P/4600/50
KH_2PO_4 (Potassium phosphate monobasic)	7778-77-0	Sigma-Aldrich	P0662
KOH (Potassium hydroxide)	1310-58-3	Sigma-Aldrich	P5958
Methanol	67-56-1	Sigma-Aldrich	M/4000/17
$MgCl_2$ (Magnesium chloride)	7786-30-3	Thermo Fisher	223211000
MOPS (4-Morpholinepropanesulfonic acid sodium salt)	71119-22-7	Alfa Aesar	A17214
Na_2HPO_4 (Sodium phosphate dibasic)	7558-79-4	Sigma-Aldrich	S5136

NaCl (Sodium chloride)	7647-14-5	Fisher Scientific	S/3160/60
NAD/NADH-Glo™ Assay	-	Promega Corporation	G9071
NADH (β-Nicotinamide adenine dinucleotide reduced)	606-68-8	Sigma-Aldrich	8129
NADPH (β-Nicotinamide adenine dinucleotide 2'-phosphate reduced tetrasodium salt)	2646-71-1	Panreac	A1395,0100
NAF (Sodium fluoride)	7681-49-4	VWR	27859.293
NaOH (Sodium hydroxide)	1310-73-2	Sigma-Aldrich	S8045
Nicotinamide	98-92-0	Sigma-Aldrich	N0636
NP40	127087-87-0	Sigma-Aldrich	NP40S
Oxaloacetate	328-42-7	Acros Organics	416600050
PhosSTOP (phosphatase inhibitor)	-	Sigma-Aldrich	4906845001
PKA kinase activity kit	-	Enzo Life Sciences	ADI-EKS-390A
PMSF (Phenylmethylsulfonyl fluoride)	329-98-6	Sigma-Aldrich	P7626
Ponceau S	6226-79-5	Sigma-Aldrich	P3504
Potassium carbonate	584-08-7	VWR	26724.291
Precision Plus ProteinTM Standard Dual Color	-	Bio-Rad	161-0374
Protease inhibitor cocktail	-	Sigma-Aldrich	P8340
QIAmp DNA mini-kit	-	Qiagen	51304
Rotenone	83-79-4	Sigma-Aldrich	R8875
SDS (Sodium dodecyl sulfate)	151-21-3	NZY tech	MB01501
SOD activity kit	-	Enzo Life Sciences	ADI-900-157
Sodium acetate	127-09-3	Sigma-Aldrich	S8750
Sodium azide	26628-22-8	Sigma-Aldrich	S2002
Sodium bicarbonate	144-55-8	Sigma-Aldrich	S6297
Sodium butyrate	156-54-7	Sigma-Aldrich	B5887
Sodium dithionite	7775-14-6	Fisher Scientific	S/3800/53
Sodium orthovanadate	13721-39-6	Sigma-Aldrich	S6508
Sodium succinate	6106-21-4	Fisher Scientific	S/6480/53
SsoFast Eva Green Supermix	-	Bio-Rad	172-5201
TEMED (1,2-Bis(dimethylamino)ethane)	110-18-9	NZY tech	MB03501
Tert-butylperoxide	110-05-4	Sigma-Aldrich	168521
Tris HCl	1185-53-1	Sigma-Aldrich	T3253
Triton X-100	9002-93-1	Acros Organics	327371000
Trizma base	77-86-1	Sigma-Aldrich	T1503
Tween-20	9005-64-5	Sigma-Aldrich	P9416
β-glycerophosphate	58409-70-4	Sigma-Aldrich	G6626
β-mercaptoethanol	60-24-2	Sigma-Aldrich	M3148

Table S2 - Composition of the diet fed to ewes throughout the study.

Ingredients	%
Ground bromegrass hay [a]	14.02
Ground corn	63.89
Soybean meal	13.30
Liquid molasses	5.60
Limestone	2.24
Ammonium chloride	0.50
Mineralized salt [b]	0.24
Magnesium chloride	0.10
ADE premix [c]	0.10
Rumensin 80	0.02

[a] Mean particle length = 2.54 cm. [b] Contained 13% NaCl, 10% Ca, 10% P, 2% K, 1.5% Mg, 0.28% Fe, 0.27% Zn, 0.12% Mn, 0.01% I, 35 p.p.m. Se, and 20 p.p.m. Co. [c] Contained 110 000 IU kg-1 vitamin A, 27 500 IU kg -1 vitamin D, 660 IU kg-1 vitamin E.

Table S3 - Nutrient analysis of the experimental diet.

Analyzed Composition	
Dry matter (%)	**88.54**
Neutral detergent fibre (% DM)	**24.09**
Acid detergent fibre (% DM)	**9.99**
Crude protein (% DM)	**17.39**
In vitro dry matter digestibility (% DM)	**93.92**

Table S4 - Sequences of the primers used for the quantification of mtDNA copy number.

Gene	Accession number	Forward primer	Reverse primer
CytB	NC_001941.1 (14159-15298)	CAGGATCCAACAACCCCACA	GTCTCCGAGTAAGTCAGGCG
YWHAZ	NM_001267887.1	GAGCAGGCTGAGCGATATGA	TGACCTACGGGCTCCTACAA

Table S5 - List of primary antibodies used to perform protein determination by Western blot. 'Accession number' represents the UniProt (The Universal Protein Resource; https://www.uniprot.org/) reference of the protein and 'dilution' corresponds to the dilution used for each antibody during incubation.

	Protein	Accession Number	Manufacture code		Host Specie	MW (kDa)	Dilution
ANT 1/2	Adenosine nucleotide translocator 1/2	P12235	Abcam	110322	Mouse	33	1:1000
ATP5a	ATP synthase subunit alpha	P25705	Mito Science	Ab110273	Mouse	54	1:500
Cat	Catalase	P04040	Mito Science	Ab14754	Mouse	48	1:1000
COX-II	Cytochrome c oxidase subunit 2	P00403	Mito Science	Ab110258	Mouse	22	1:500
CS	Citrate synthase	O75390	Santa Cruz	390693	Mouse	58	1:1000
CVα	ATP synthase subunit alpha	P05496	Mito Science	Ab14748	Mouse	55	1:1000
GPx-1	Glutathione peroxidase 1	P07203	Santa Cruz	133160	Mouse	23	1:500
GPx-4	Glutathione peroxidase 4	P36969	Santa Cruz	166570	Mouse	21	1:500
GR	Glutathione Reductase	P00390	Santa Cruz	133245	Mouse	50	1:1000
mtCO1	Cytochrome c oxidase subunit 1	P00395	Abcam	14705	Mouse	57	1:1000
Ndufs8	NADH dehydrogenase iron-sulfur protein 8	O00217	Mito Science	Ab110242	Mouse	18	1:1000
PGC-1α	Peroxisome proliferator-activated receptor gamma coactivator 1-alpha	Q9UBK2	Santa Cruz	13067	Rabbit	90	1:500
PKA	cAMP-dependent protein kinase catalytic subunit alpha	P17612	Santa Cruz	28892	Rabbit	40	1:1000
PPARγ	Peroxisome proliferator-activated receptor gamma	P37231	Abcam	41928	Mouse	58	1:1000
SDHA	Succinate dehydrogenase flavoprotein subunit	P31040	Santa Cruz	59687	Mouse	70	1:1000
SDHB	Succinate dehydrogenase iron-sulfur subunit	P21912	Mito Science	Ab14714	Mouse	29	1:500
TOM 20	Mitochondrial import receptor subunit TOM20	Q15388	Santa Cruz	49760	Rabbit	20	1:1000
UQCRC1	Cytochrome b-c1 complex subunit 1	P31930	Mito Science	Ab110252	Mouse	49	1:500
UQCRC2	Cytochrome b-c1	P22695	Mito	Ab14754	Mouse	48	1:1000

	complex subunit 2		Science				
UQCRFS1	Cytochrome b-c1 complex subunit Rieske	P47985	Abcam	Ab14746	Mouse	25	1:500
VDAC	Voltage-dependent anion-selective channel protein 1	P21796	Mito Science	Ab14734	Mouse	39	1:500
β-actin		P68133	Millipore	MAB1501	Mouse	43	1:5000

Table S6 - List of secondary antibodies used in Western blot. 'Dilution' corresponds to the dilution used for each antibody during incubation.

Antibody	Description	Manufacturer Code		Host specie	Dilution
Anti-Goat	rabbit@goat	Santa Cruz	2771	Rabbit	1:5000
Anti-Mouse	goat@mouse	Santa Cruz	2008	Goat	1:5000
Anti-Rabbit	goat@rabbit	Santa Cruz	2007	Goat	1:5000

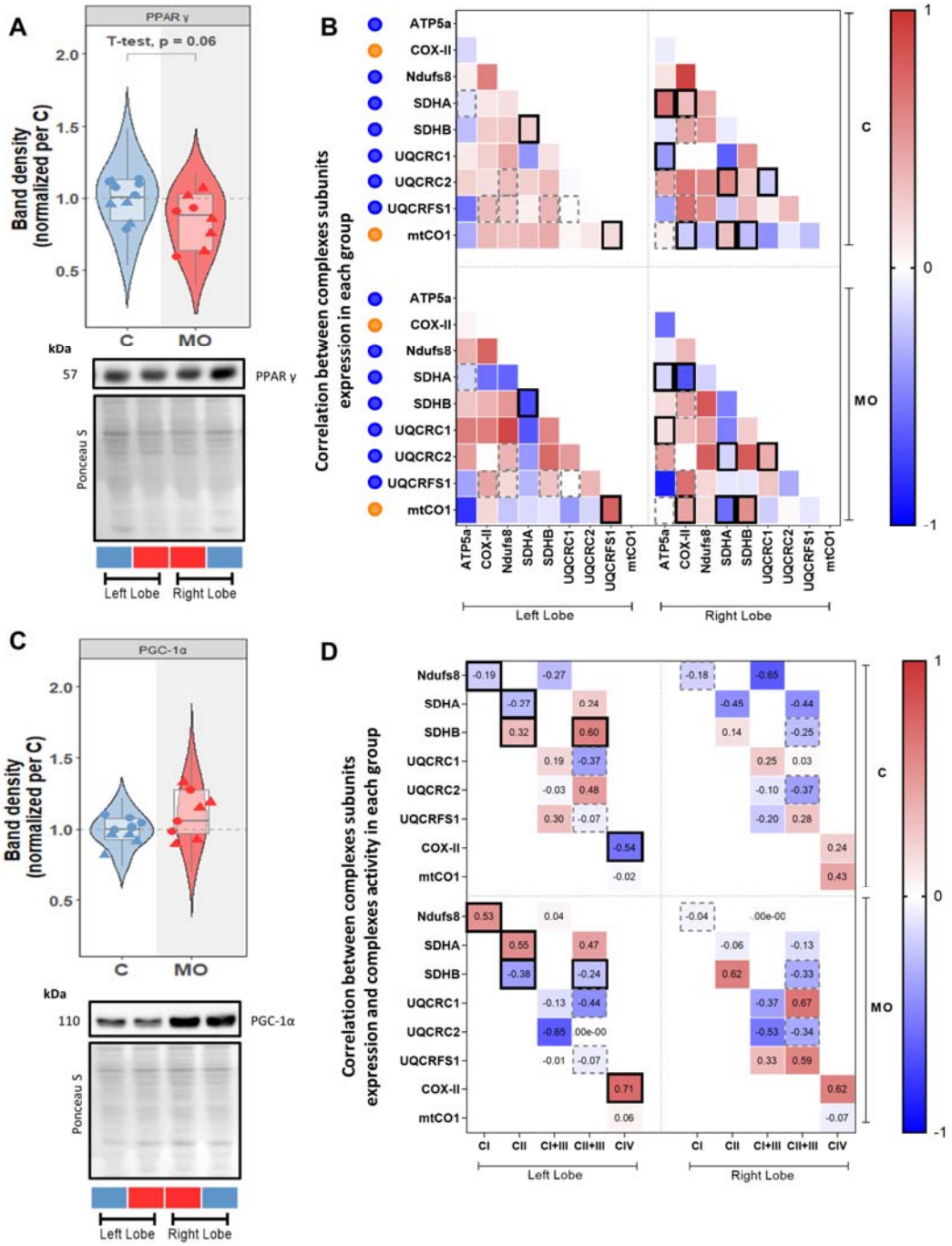

Figure S1 - Protein expression of transcription regulators of hepatic metabolism and correlations of hepatic mitochondrial respiratory chain subunits protein expression and enzymatic activity in Control (C) and Maternal obesity (MO) groups. **A:** Protein expression of PPAR γ. **B:** Correlation between complexes subunits protein expression in C and MO in each lobe. Circles show the nuclear (blue) or mitochondrial (orange) encoded origin of each subunit. Bordered correlations highlight the top ten correlations with the largest difference between correlations in C and MO of the respective lobe. Dashed rectangles depict the ten correlations with the lowest variation. **C:** Protein expression of PGC-1α. **D:** Correlation between complexes subunits protein expression and the complexes' enzymatic activity. Surrounded rectangles represent the five most significant differences between C and MO. Dashed lines highlight the correlations with the lowest difference. A correlation value of +1 indicated a total positive linear correlation, −1 a total negative correlation, and 0 identifies the inexistence of linear correlation.

Statistical analysis: Comparison between C and MO groups was performed using the unpaired t-test. P-values lower than 0.10 were registered. Blue violin plot, C; Red violin plot, MO. Median, interquartile distance, minimum and maximum are depicted. Circles represent that the mother was pregnant with male fetuses and triangles female fetuses.

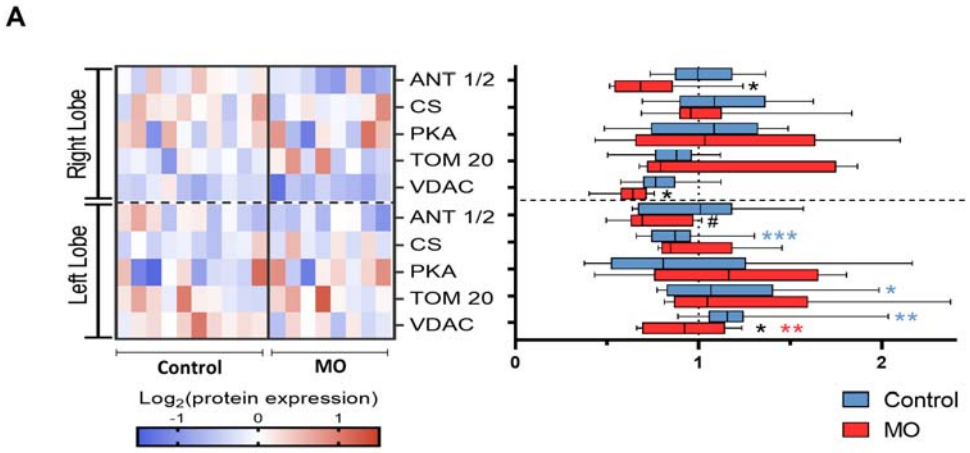

Figure S2 - Hepatic metabolic-related protein expression modulation by maternal obesity during pregnancy. **A:** Protein levels of ANT 1/2, Citrate Synthase, Protein Kinase A, TOM 20, and VDAC in each lobe in Control (C) and Maternal Obesity (MO). Protein expression was obtained by Western blot, shown in the heat map on the left (lower expression – blue, higher expression – red, unaltered expression – white). The respective boxplot is represented on the right (Control – blue, MO – red). The statistics in black represent the comparison between C and MO in the same liver lobe, in blue the comparison between both lobes of control samples, and in red between both lobes of MO. The group's average replaced missing values in the heatmap but was not considered for the boxplot and statistics.
Statistical analysis: Comparison between control and MO groups was performed using unpaired t-test, after passing Shapiro-Wilk normality test, except for the comparison in the left lobe of VDAC protein expression in which the Mann Whitney test was used. Comparison between lobes was assessed using the Wilcoxon test except for VDAC (in MO) and CS (in control) protein expression, in which the unpaired t-test was performed. P-values lower than 0.10 were registered (#) and lower than 0.05 were considered significant (* $p \leq 0.05$; ** $p \leq 0.01$; *** $p \leq 0.001$).

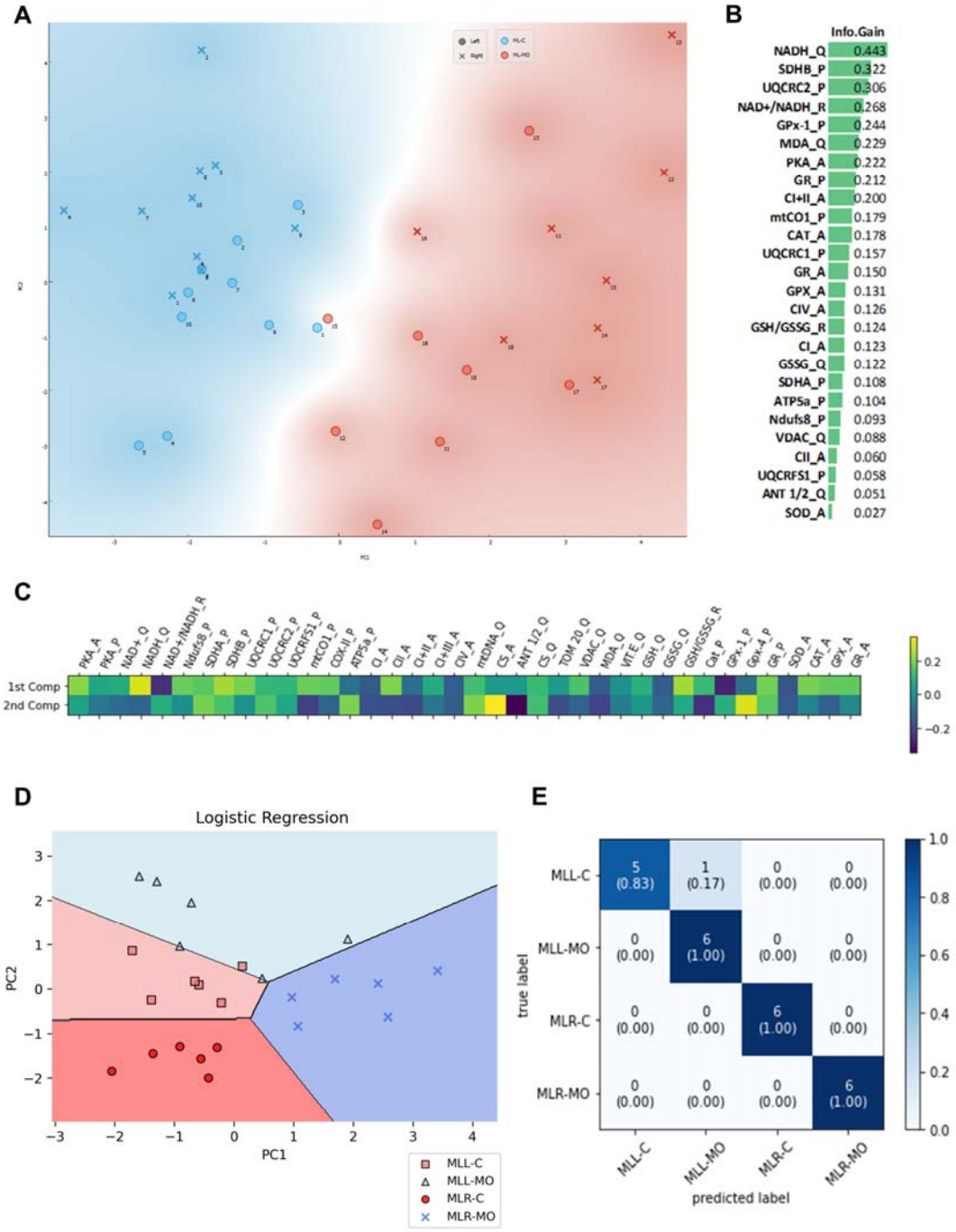

Figure S3 - Distribution of the results according to integrative data analysis. **A:** PCA of all measured parameters and samples. Control samples (blue) and Maternal Obesity (MO) samples (red) present a great separation. Each number represents the animal, circles are used for the left liver lobe samples and crosses for the right liver lobe samples. **B:** Information gain obtained for each parameter based on the comparison C vs. MO. **C:** Parameters weight in each component of the PCA for the dataset restricted to 24 samples. **D:** Evaluation of the sample's distribution based on the PCA restricted to 24 samples and the five most informative parameters through a logistic regression algorithm. **E:** Confusion matrix with the comparison of the predicted and the observed results of the distribution of samples according to the condition, based on the logistic regression algorithm. Each parameter is named using the feature analyzed followed by the type of the assay (P stands for protein quantification, A for activity, Q for quantification, and R for ratio).

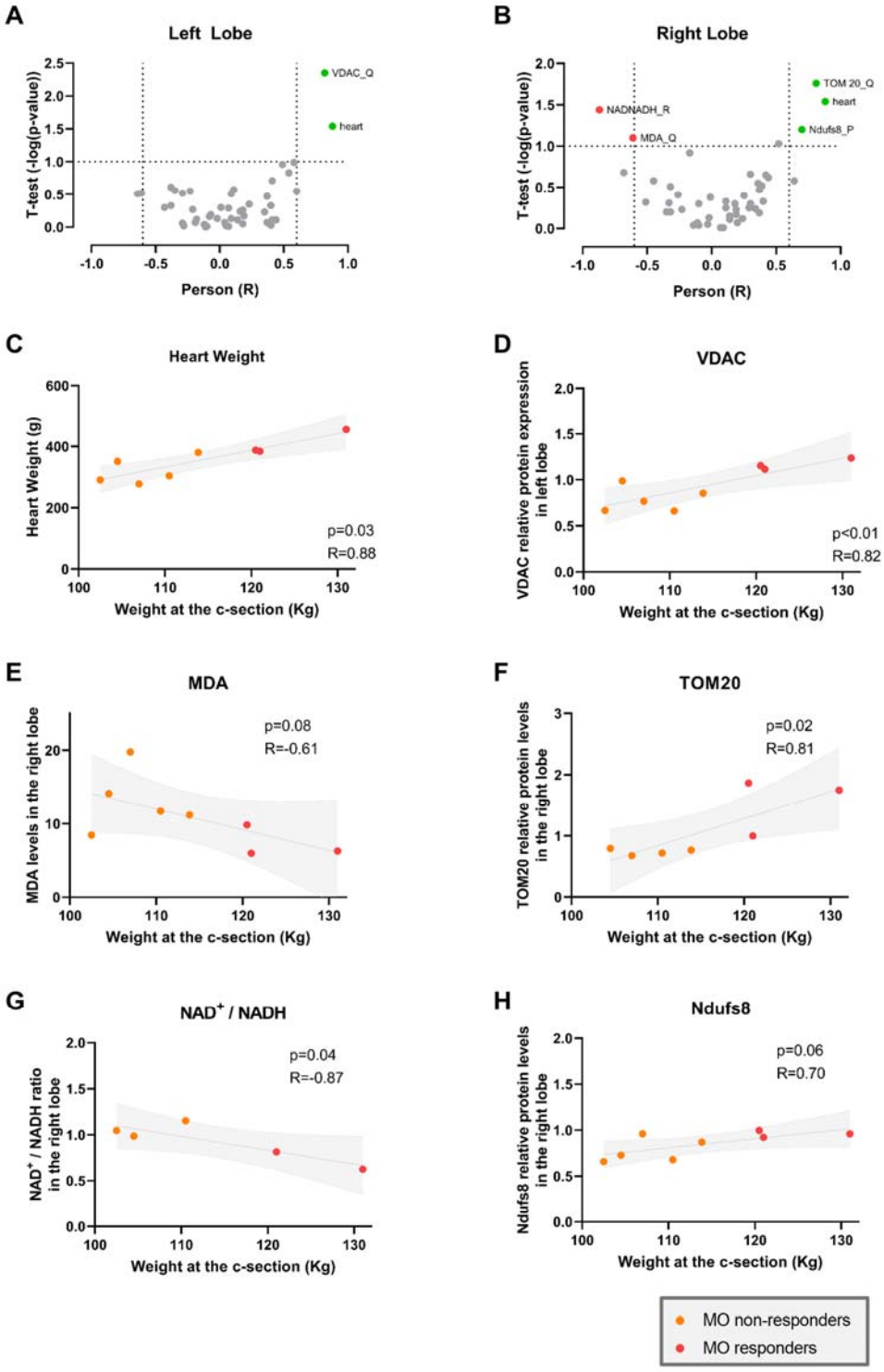

Figure S4 – Bimodal pattern of weight at c-section in the Maternal Obesity (MO) group. **A:** Comparison of responders and non-responders in the MO group based on the p-value of unpaired t-test and Pearson correlation with weight at the c-section for the left liver lobe, **B:** and for the right liver lobe. Correlation between weight at the c-section and the significant parameters: **C:** Heart weight, **D:** VDAC, **E:** MDA, **F:** TOM20, **G:** NAD^+ / NADH, and **H:** Ndufs8.

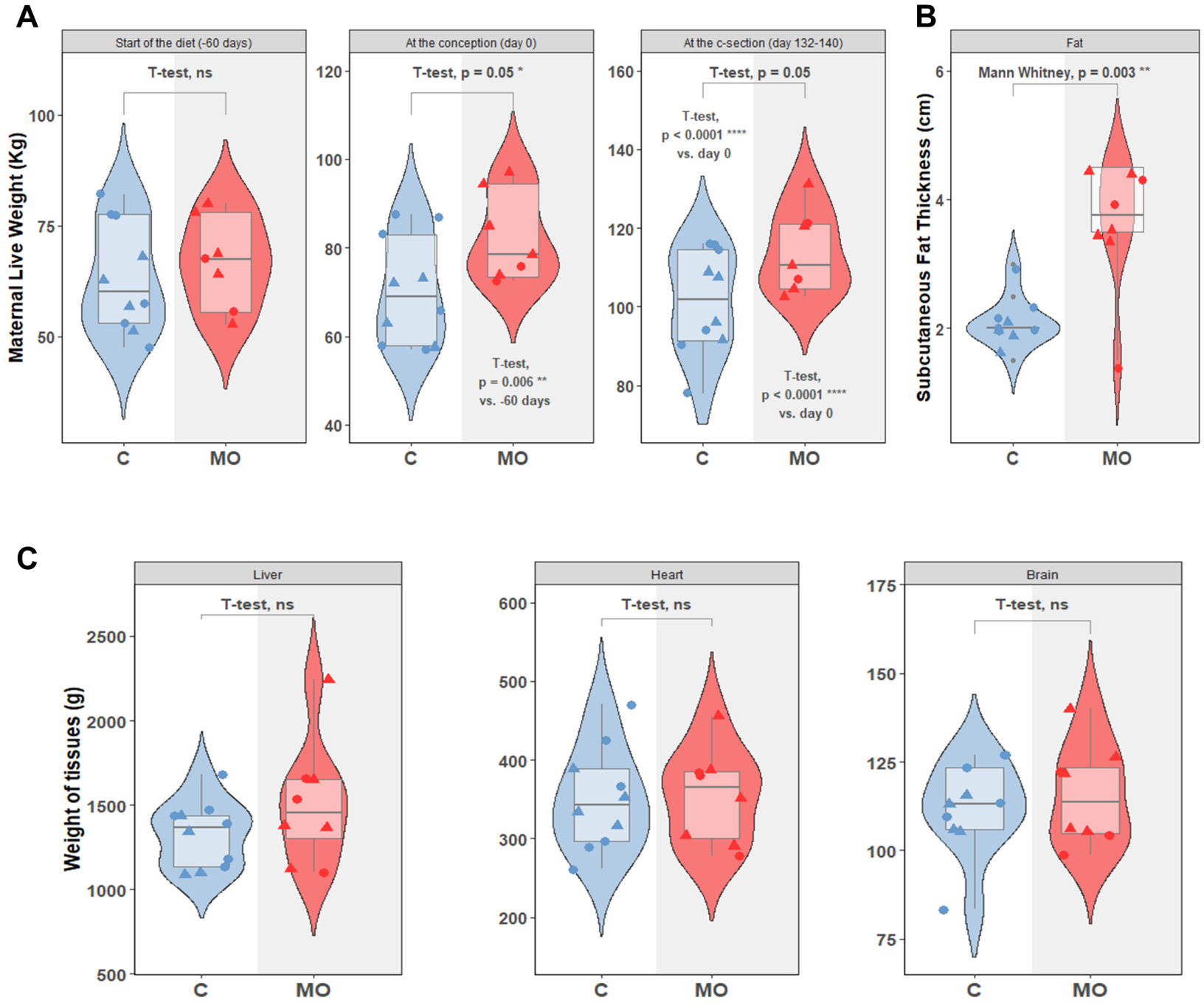
A
Start of the diet (-60 days)
T-test, ns
At the conception (day 0)
T-test, p = 0.05 *
T-test,
p = 0.006 **
vs. -60 days
At the c-section (day 132-140)
T-test, p = 0.05
T-test,
p < 0.0001 ****
vs. day 0
T-test,
p < 0.0001 ****
vs. day 0
Maternal Live Weight (Kg)
C
MO
B
Fat
Mann Whitney, p = 0.003 **
Subcutaneous Fat Thickness (cm)
C
MO
C
Liver
T-test, ns
Heart
T-test, ns
Brain
T-test, ns
Weight of tissues (g)
C
MO
C
MO
C
MO

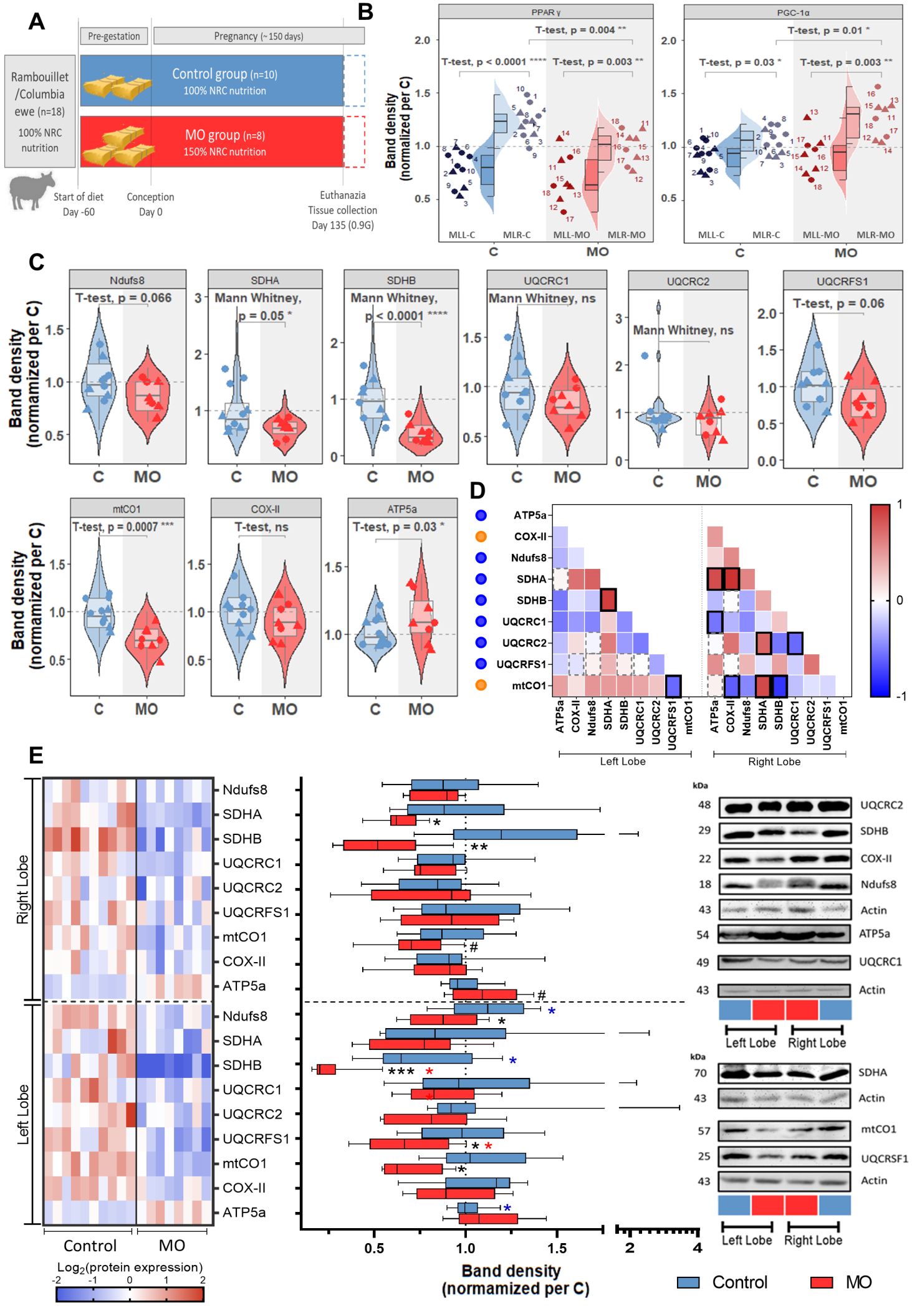
A
Pre-gestation
Pregnancy (~150 days)
Rambouillet /Columbia ewe (n=18)
100% NRC nutrition
Control group (n=10)
100% NRC nutrition
MO group (n=8)
150% NRC nutrition
Start of diet Day -60
Conception Day 0
Euthanazia Tissue collection Day 135 (0.9G)
B
PPARγ
T-test, p = 0.004 **
T-test, p < 0.0001 ****
T-test, p = 0.003 **
PGC-1α
T-test, p = 0.01 *
T-test, p = 0.03 *
T-test, p = 0.003 **
Band density (normalized per C)
MLL-C
MLR-C
MLL-MO
MLR-MO
C
MO
C
Ndufs8
T-test, p = 0.066
SDHA
Mann Whitney, p = 0.05 *
SDHB
Mann Whitney, p < 0.0001 ****
UQCRC1
Mann Whitney, ns
UQCRC2
Mann Whitney, ns
UQCRFS1
T-test, p = 0.06
mtCO1
T-test, p = 0.0007 ***
COX-II
T-test, ns
ATP5a
T-test, p = 0.03 *
D
ATP5a
COX-II
Ndufs8
SDHA
SDHB
UQCRC1
UQCRC2
UQCRFS1
mtCO1
Left Lobe
Right Lobe
E
Right Lobe
Left Lobe
Control
MO
Log2(protein expression)
Band density (normarized per C)
kDa
UQCRC2
SDHB
COX-II
Ndufs8
Actin
ATP5a
UQCRC1
SDHA
mtCO1
UQCRSF1

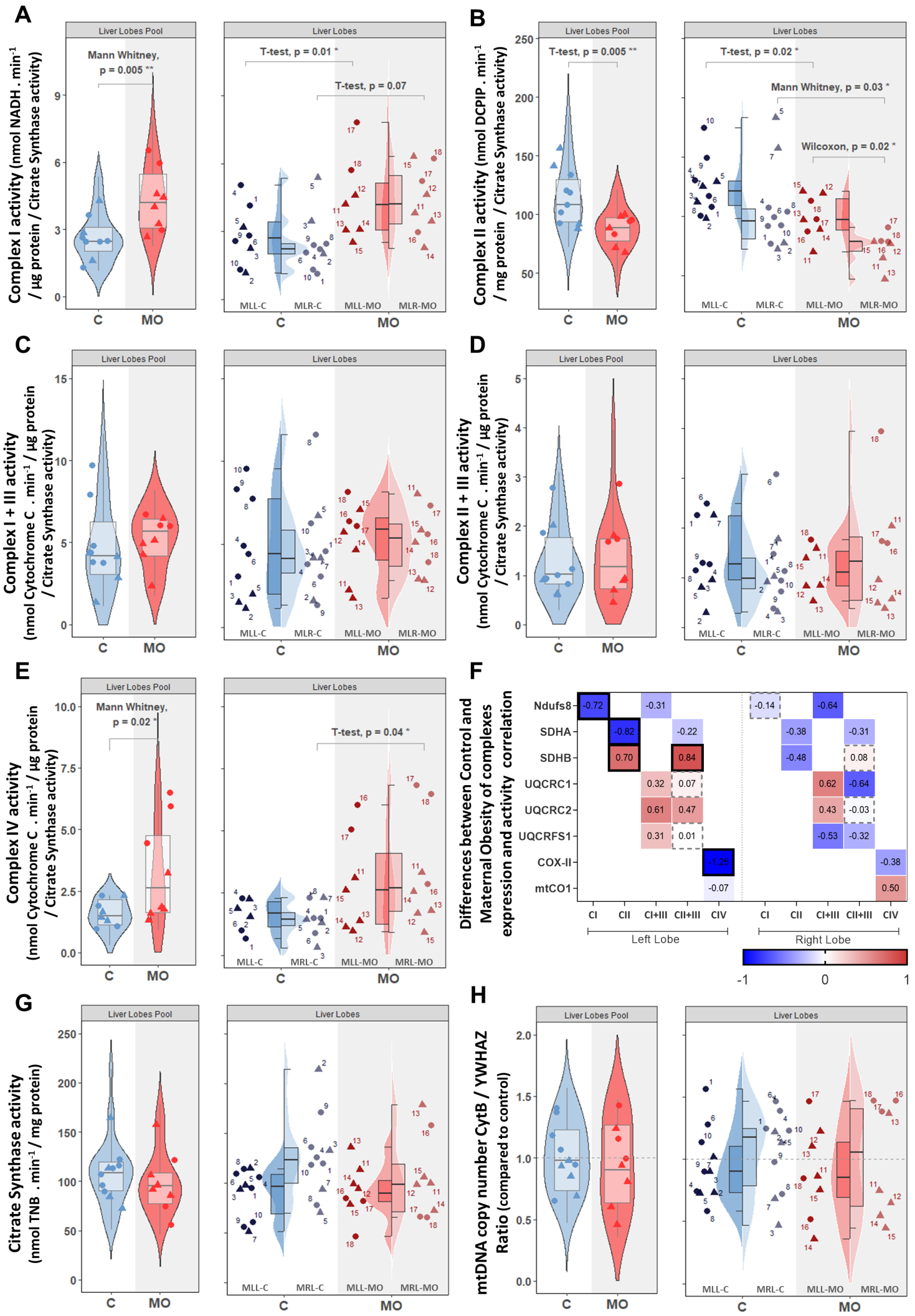
A
Complex I activity (nmol NADH . min-1 / µg protein / Citrate Synthase activity)
Liver Lobes Pool
Mann Whitney, p = 0.005 **
Liver Lobes
T-test, p = 0.01 *
T-test, p = 0.07
C
MO
MLL-C
MLR-C
MLL-MO
MLR-MO
B
Complex II activity (nmol DCPIP . min-1 / mg protein / Citrate Synthase activity)
T-test, p = 0.005 **
T-test, p = 0.02 *
Mann Whitney, p = 0.03 *
Wilcoxon, p = 0.02 *
C
Complex I + III activity (nmol Cytochrome C . min-1 / µg protein / Citrate Synthase activity)
D
Complex II + III activity (nmol Cytochrome C . min-1 / µg protein / Citrate Synthase activity)
E
Complex IV activity (nmol Cytochrome C . min-1 / µg protein / Citrate Synthase activity)
Mann Whitney, p = 0.02 *
T-test, p = 0.04 *
F
Differences between Control and Maternal Obesity of complexes expression and activity correlation
Ndufs8
SDHA
SDHB
UQCRC1
UQCRC2
UQCRFS1
COX-II
mtCO1
CI
CII
CI+III
CII+III
CIV
Left Lobe
Right Lobe
-1
0
1
G
Citrate Synthase activity (nmol TNB . min-1 / mg protein)
H
mtDNA copy number CytB / YWHAZ Ratio (compared to control)

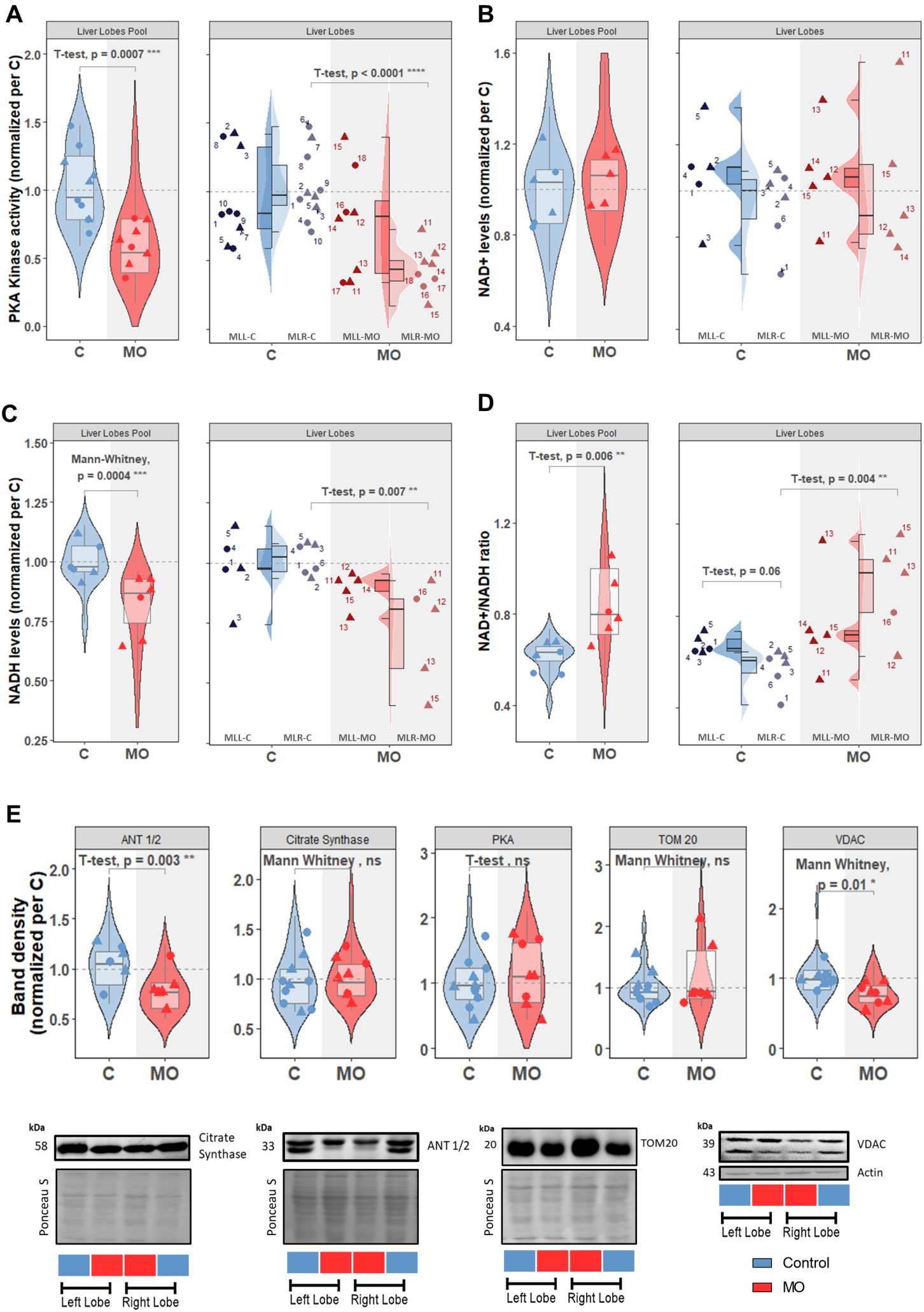
A
Liver Lobes Pool
T-test, p = 0.0007 ***
PKA Kinase activity (normalized per C)
C
MO
Liver Lobes
T-test, p < 0.0001 ****
MLL-C
MLR-C
MLL-MO
MLR-MO
B
Liver Lobes Pool
NAD+ levels (normalized per C)
Liver Lobes
C
D
Liver Lobes Pool
T-test, p = 0.006 **
NAD+/NADH ratio
Liver Lobes
T-test, p = 0.004 **
T-test, p = 0.06
E
ANT 1/2
T-test, p = 0.003 **
Band density (normalized per C)
Citrate Synthase
Mann Whitney , ns
PKA
T-test , ns
TOM 20
Mann Whitney, ns
VDAC
Mann Whitney, p = 0.01 *
kDa
58
Citrate Synthase
Ponceau S
Left Lobe
Right Lobe
33
ANT 1/2
20
TOM20
39
VDAC
43
Actin
Control
MO

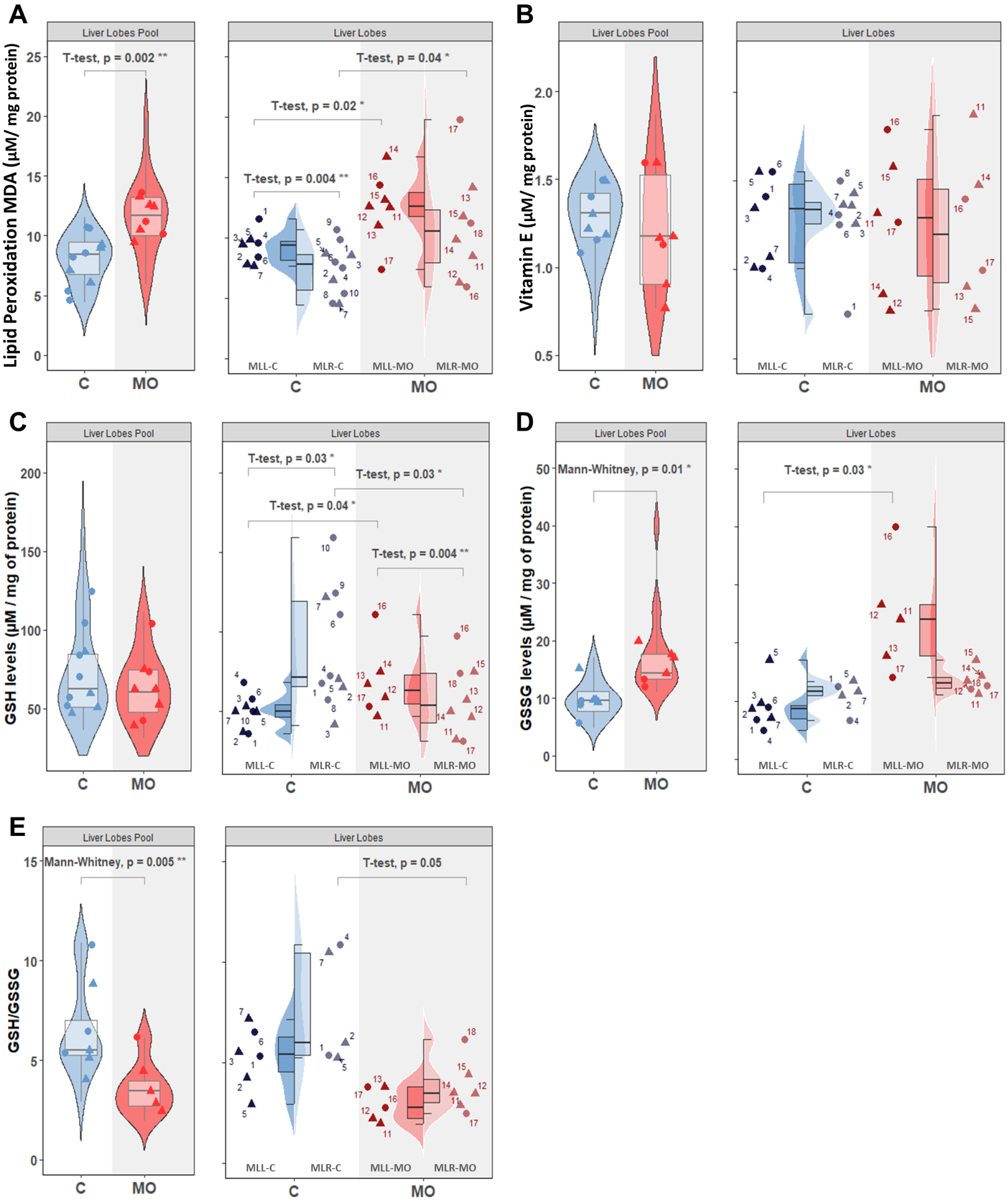
A
Liver Lobes Pool
Liver Lobes
Lipid Peroxidation MDA (µM/ mg protein)
T-test, p = 0.002 **
T-test, p = 0.04 *
T-test, p = 0.02 *
T-test, p = 0.004 **
B
Vitamin E (µM/ mg protein)
C
Mann-Whitney, p = 0.01 *
T-test, p = 0.03 *
GSH levels (µM / mg of protein)
GSSG levels (µM / mg of protein)
D
T-test, p = 0.03 *
T-test, p = 0.04 *
T-test, p = 0.004 **
E
GSH/GSSG
Mann-Whitney, p = 0.005 **
T-test, p = 0.05
C
MO
MLL-C
MLR-C
MLL-MO
MLR-MO

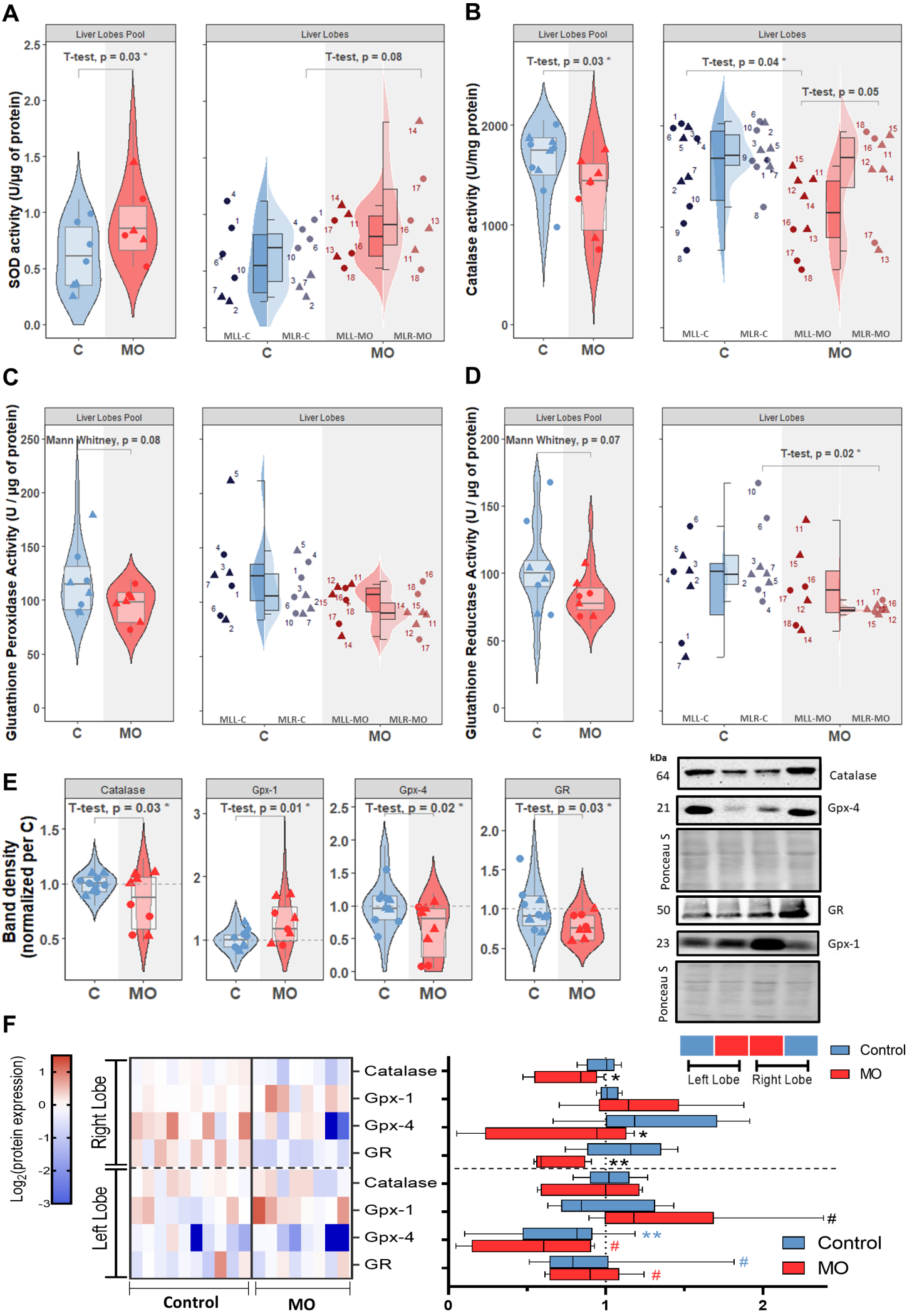
A
Liver Lobes Pool
T-test, p = 0.03 *
SOD activity (U/µg of protein)
C
MO
Liver Lobes
T-test, p = 0.08
MLL-C
MLR-C
MLL-MO
MLR-MO
B
Liver Lobes Pool
T-test, p = 0.03 *
Catalase activity (U/mg protein)
Liver Lobes
T-test, p = 0.04 *
T-test, p = 0.05
C
Glutathione Peroxidase Activity (U / µg of protein)
Mann Whitney, p = 0.08
D
Glutathione Reductase Activity (U / µg of protein)
Mann Whitney, p = 0.07
T-test, p = 0.02 *
E
Band density (normalized per C)
Catalase
T-test, p = 0.03 *
Gpx-1
T-test, p = 0.01 *
Gpx-4
T-test, p = 0.02 *
GR
T-test, p = 0.03 *
kDa
64
Catalase
21
Gpx-4
Ponceau S
50
GR
23
Gpx-1
Ponceau S
F
Log2(protein expression)
Right Lobe
Left Lobe
Catalase
Gpx-1
Gpx-4
GR
Control
MO
Left Lobe
Right Lobe
Control
MO

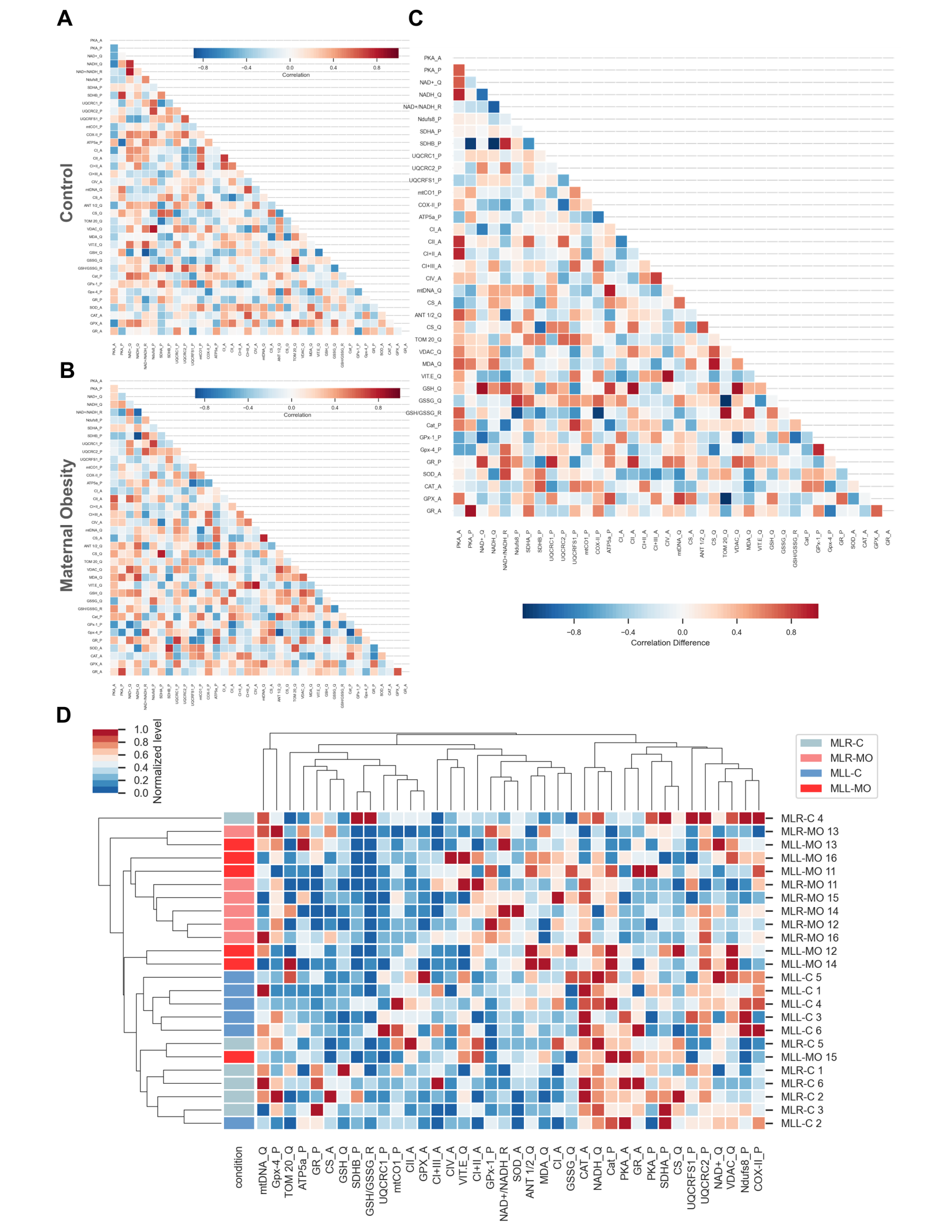
A
Control
B
Maternal Obesity
Correlation
−0.8
−0.4
0.0
0.4
0.8
C
Correlation Difference
D
Normalized level
1.0
0.8
0.6
0.4
0.2
0.0
MLR-C
MLR-MO
MLL-C
MLL-MO
MLR-C 4
MLR-MO 13
MLL-MO 13
MLL-MO 16
MLL-MO 11
MLR-MO 11
MLR-MO 15
MLR-MO 14
MLR-MO 12
MLR-MO 16
MLL-MO 12
MLL-MO 14
MLL-C 5
MLL-C 1
MLL-C 4
MLL-C 3
MLL-C 6
MLR-C 5
MLL-MO 15
MLR-C 1
MLR-C 6
MLR-C 2
MLR-C 3
MLL-C 2
condition
mtDNA_Q
Gpx-4_P
TOM 20_Q
ATP5a_P
GR_P
CS_A
GSH_Q
SDHB_P
GSH/GSSG_R
UQCRC1_P
mtCO1_P
CII_A
GPX_A
CI+III_A
CIV_A
VIT.E_Q
CI+II_A
GPx-1_P
NAD+/NADH_R
SOD_A
ANT 1/2_Q
MDA_Q
CI_A
GSSG_Q
CAT_A
NADH_Q
Cat_P
PKA_A
GR_A
PKA_P
SDHA_P
CS_Q
UQCRFS1_P
UQCRC2_P
NAD+_Q
VDAC_Q
Ndufs8_P
COX-II_P

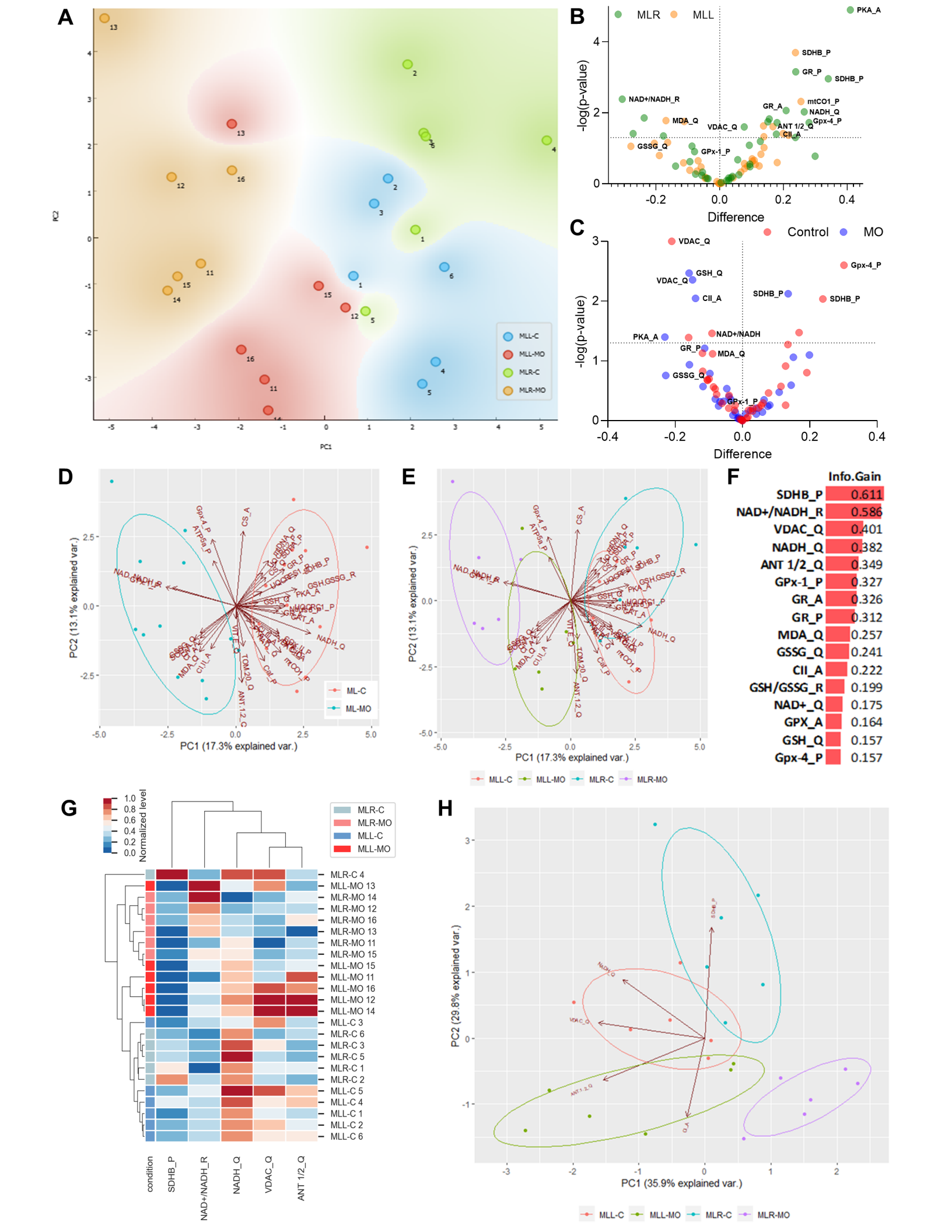
A
MLL-C
MLL-MO
MLR-C
MLR-MO
PC1
PC2
B
MLR
MLL
-log(p-value)
Difference
PKA_A
SDHB_P
GR_P
SDHB_P
NAD+/NADH_R
mtCO1_P
GR_A
NADH_Q
MDA_Q
VDAC_Q
ANT 1/2_Q
Gpx-4_P
CII_A
GSSG_Q
GPx-1_P
C
Control
MO
-log(p-value)
Difference
VDAC_Q
Gpx-4_P
GSH_Q
VDAC_Q
CII_A
SDHB_P
SDHB_P
PKA_A
NAD+/NADH
GR_P
MDA_Q
GSSG_Q
GPx-1_P
D
PC2 (13.1% explained var.)
PC1 (17.3% explained var.)
ML-C
ML-MO
E
PC2 (13.1% explained var.)
PC1 (17.3% explained var.)
MLL-C
MLL-MO
MLR-C
MLR-MO
F
Info.Gain
SDHB_P 0.611
NAD+/NADH_R 0.586
VDAC_Q 0.401
NADH_Q 0.382
ANT 1/2_Q 0.349
GPx-1_P 0.327
GR_A 0.326
GR_P 0.312
MDA_Q 0.257
GSSG_Q 0.241
CII_A 0.222
GSH/GSSG_R 0.199
NAD+_Q 0.175
GPX_A 0.164
GSH_Q 0.157
Gpx-4_P 0.157
G
Normalized level
MLR-C
MLR-MO
MLL-C
MLL-MO
MLR-C 4
MLL-MO 13
MLR-MO 14
MLR-MO 12
MLR-MO 16
MLR-MO 13
MLR-MO 11
MLR-MO 15
MLL-MO 15
MLL-MO 11
MLL-MO 16
MLL-MO 12
MLL-MO 14
MLL-C 3
MLR-C 6
MLR-C 3
MLR-C 5
MLR-C 1
MLR-C 2
MLL-C 5
MLL-C 4
MLL-C 1
MLL-C 2
MLL-C 6
condition
SDHB_P
NAD+/NADH_R
NADH_Q
VDAC_Q
ANT 1/2_Q
H
PC2 (29.8% explained var.)
PC1 (35.9% explained var.)
MLL-C
MLL-MO
MLR-C
MLR-MO

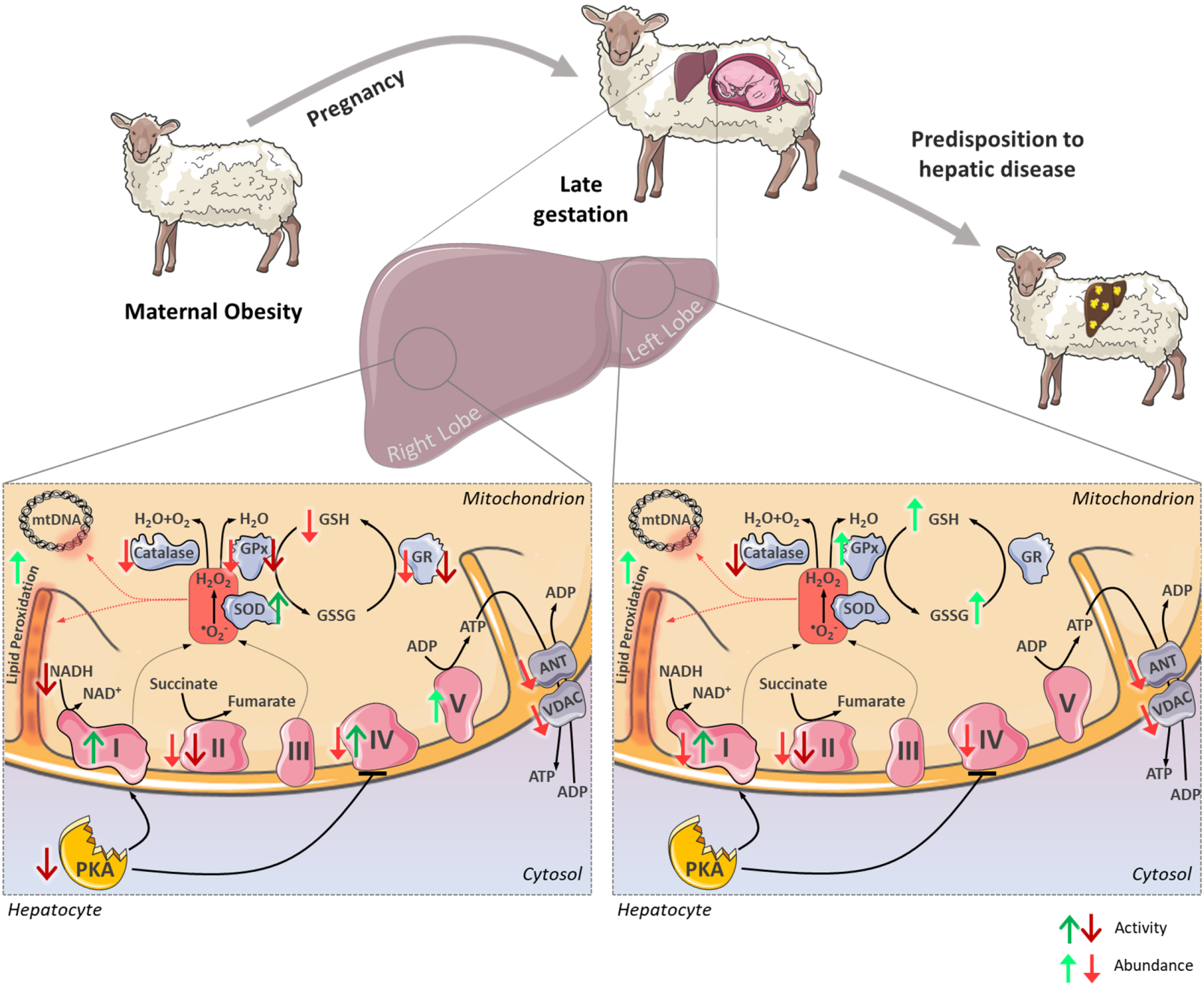
Pregnancy
Late gestation
Predisposition to hepatic disease
Maternal Obesity
Left Lobe
Right Lobe
Mitochondrion
mtDNA
Lipid Peroxidation
Catalase
GPx
GR
SOD
GSH
GSSG
NADH
NAD+
Succinate
Fumarate
ATP
ADP
ANT
VDAC
PKA
Cytosol
Hepatocyte
Activity
Abundance

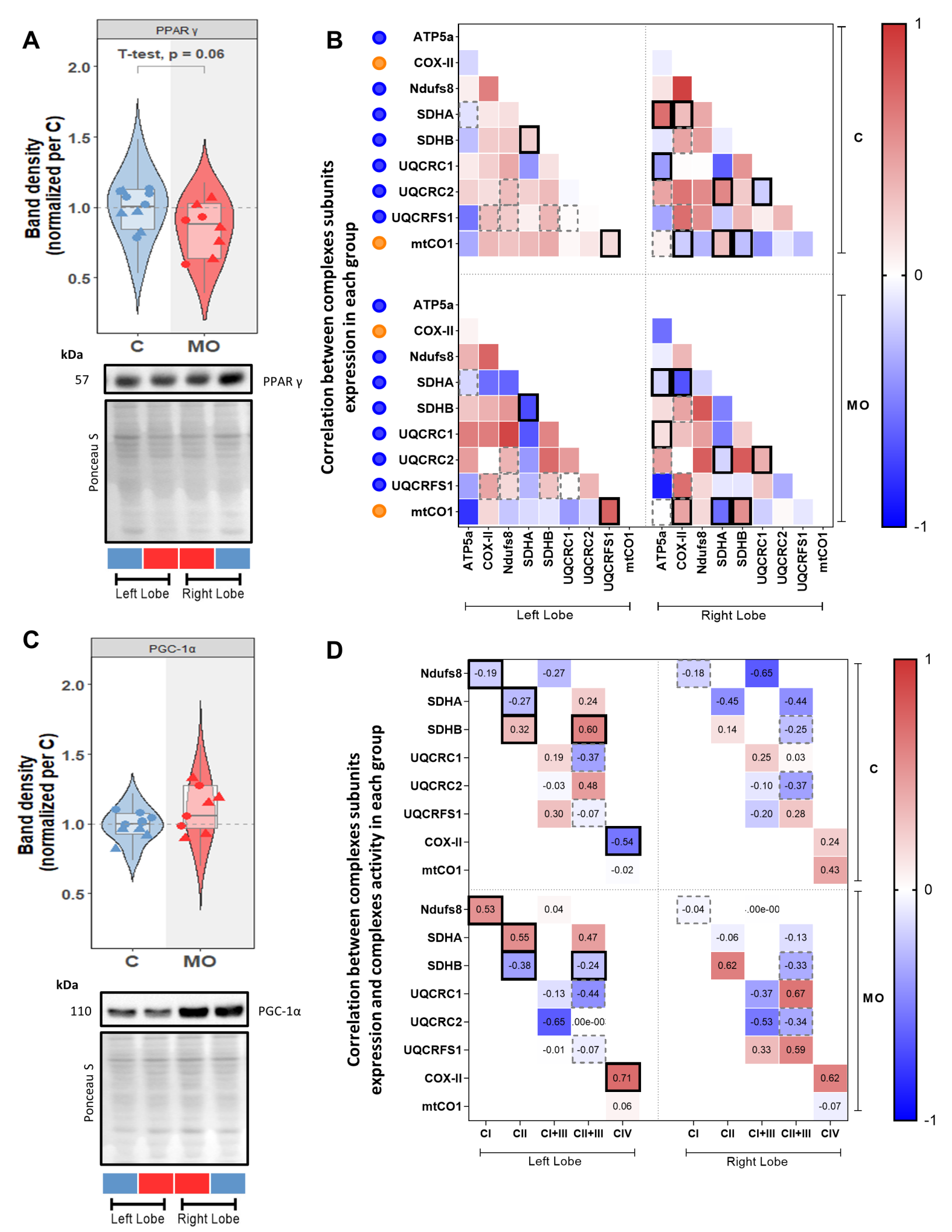
A
PPAR γ
T-test, p = 0.06
Band density (normalized per C)
2.0
1.5
1.0
0.5
C
MO
kDa
57
PPAR γ
Ponceau S
Left Lobe
Right Lobe
B
Correlation between complexes subunits expression in each group
ATP5a
COX-II
Ndufs8
SDHA
SDHB
UQCRC1
UQCRC2
UQCRFS1
mtCO1
C
MO
Left Lobe
Right Lobe
1
0
-1
C
PGC-1α
Band density (normalized per C)
2.0
1.5
1.0
0.5
C
MO
kDa
110
PGC-1α
Ponceau S
Left Lobe
Right Lobe
D
Correlation between complexes subunits expression and complexes activity in each group
Ndufs8
SDHA
SDHB
UQCRC1
UQCRC2
UQCRFS1
COX-II
mtCO1
-0.19
-0.27
0.24
-0.27
0.32
0.60
0.19
-0.37
-0.03
0.48
0.30
-0.07
-0.54
-0.02
-0.18
-0.65
-0.45
-0.44
0.14
-0.25
0.25
0.03
-0.10
-0.37
-0.20
0.28
0.24
0.43
0.53
0.04
0.55
0.47
-0.38
-0.24
-0.13
-0.44
-0.65
.00e-00
-0.01
-0.07
0.71
0.06
-0.04
.00e-00
-0.06
-0.13
0.62
-0.33
-0.37
0.67
-0.53
-0.34
0.33
0.59
0.62
-0.07
CI
CII
CI+III
CII+III
CIV
Left Lobe
Right Lobe
C
MO
1
0
-1

A

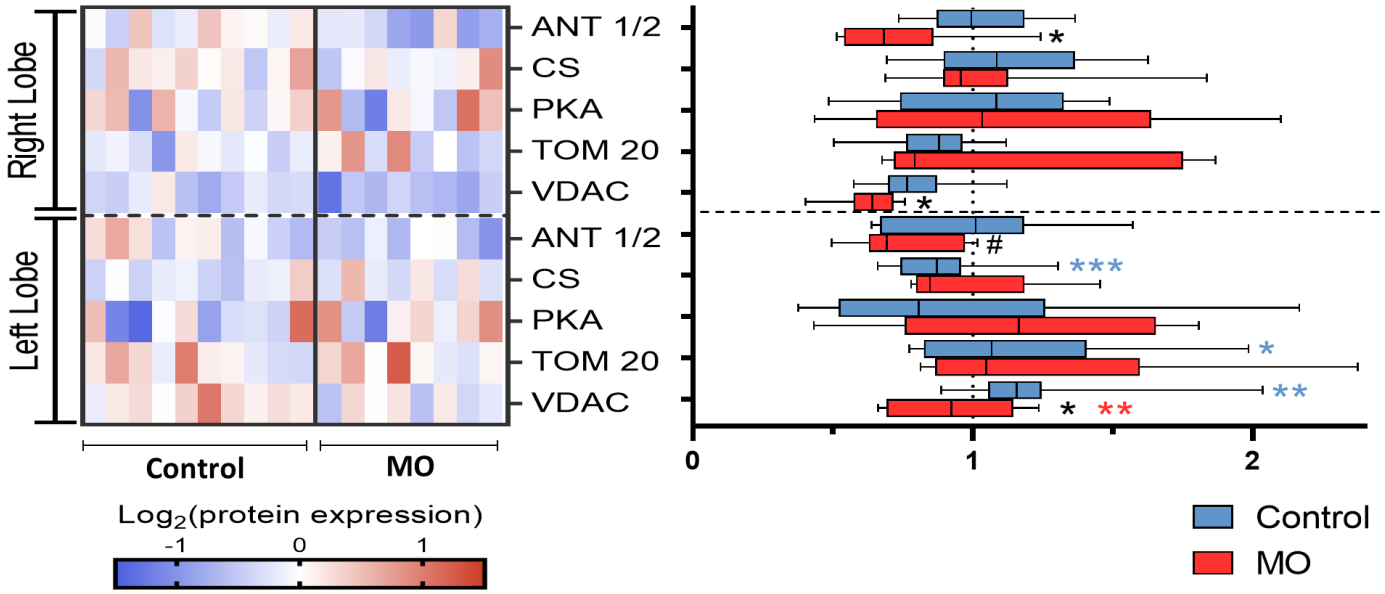
Right Lobe
Left Lobe
ANT 1/2
CS
PKA
TOM 20
VDAC
ANT 1/2
CS
PKA
TOM 20
VDAC
Control
MO
Log2(protein expression)
-1
0
1
0
1
2
Control
MO

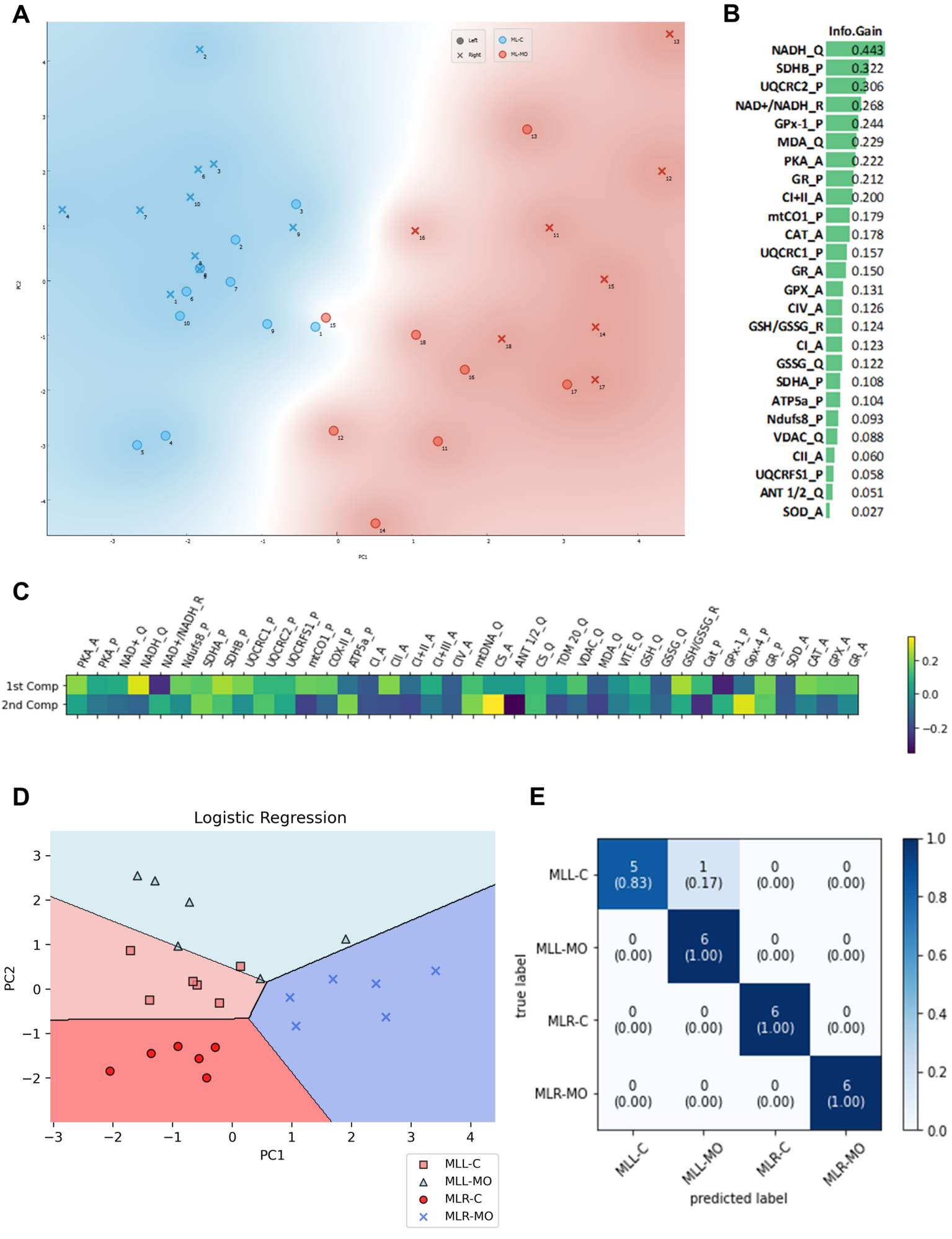
A
Left
Right
ML-C
ML-MO
PC1
PC2
B
Info.Gain
NADH_Q 0.443
SDHB_P 0.322
UQCRC2_P 0.306
NAD+/NADH_R 0.268
GPx-1_P 0.244
MDA_Q 0.229
PKA_A 0.222
GR_P 0.212
CI+II_A 0.200
mtCO1_P 0.179
CAT_A 0.178
UQCRC1_P 0.157
GR_A 0.150
GPX_A 0.131
CIV_A 0.126
GSH/GSSG_R 0.124
CI_A 0.123
GSSG_Q 0.122
SDHA_P 0.108
ATP5a_P 0.104
Ndufs8_P 0.093
VDAC_Q 0.088
CII_A 0.060
UQCRFS1_P 0.058
ANT 1/2_Q 0.051
SOD_A 0.027
C
PKA_A
PKA_P
NAD+_Q
NADH_Q
NAD+/NADH_R
Ndufs8_P
SDHA_P
SDHB_P
UQCRC1_P
UQCRC2_P
UQCRFS1_P
mtCO1_P
COX-II_P
ATP5a_P
CI_A
CII_A
CI+II_A
CI+III_A
CIV_A
mtDNA_Q
CS_A
ANT 1/2_Q
CS_Q
TOM 20_Q
VDAC_Q
MDA_Q
VIT.E_Q
GSH_Q
GSSG_Q
GSH/GSSG_R
Cat_P
GPx-1_P
Gpx-4_P
GR_P
SOD_A
CAT_A
GPX_A
GR_A
1st Comp
2nd Comp
0.2
0.0
−0.2
D
Logistic Regression
PC1
PC2
MLL-C
MLL-MO
MLR-C
MLR-MO
E
true label
predicted label
MLL-C
MLL-MO
MLR-C
MLR-MO
5 (0.83)
1 (0.17)
0 (0.00)
6 (1.00)
1.0
0.8
0.6
0.4
0.2
0.0

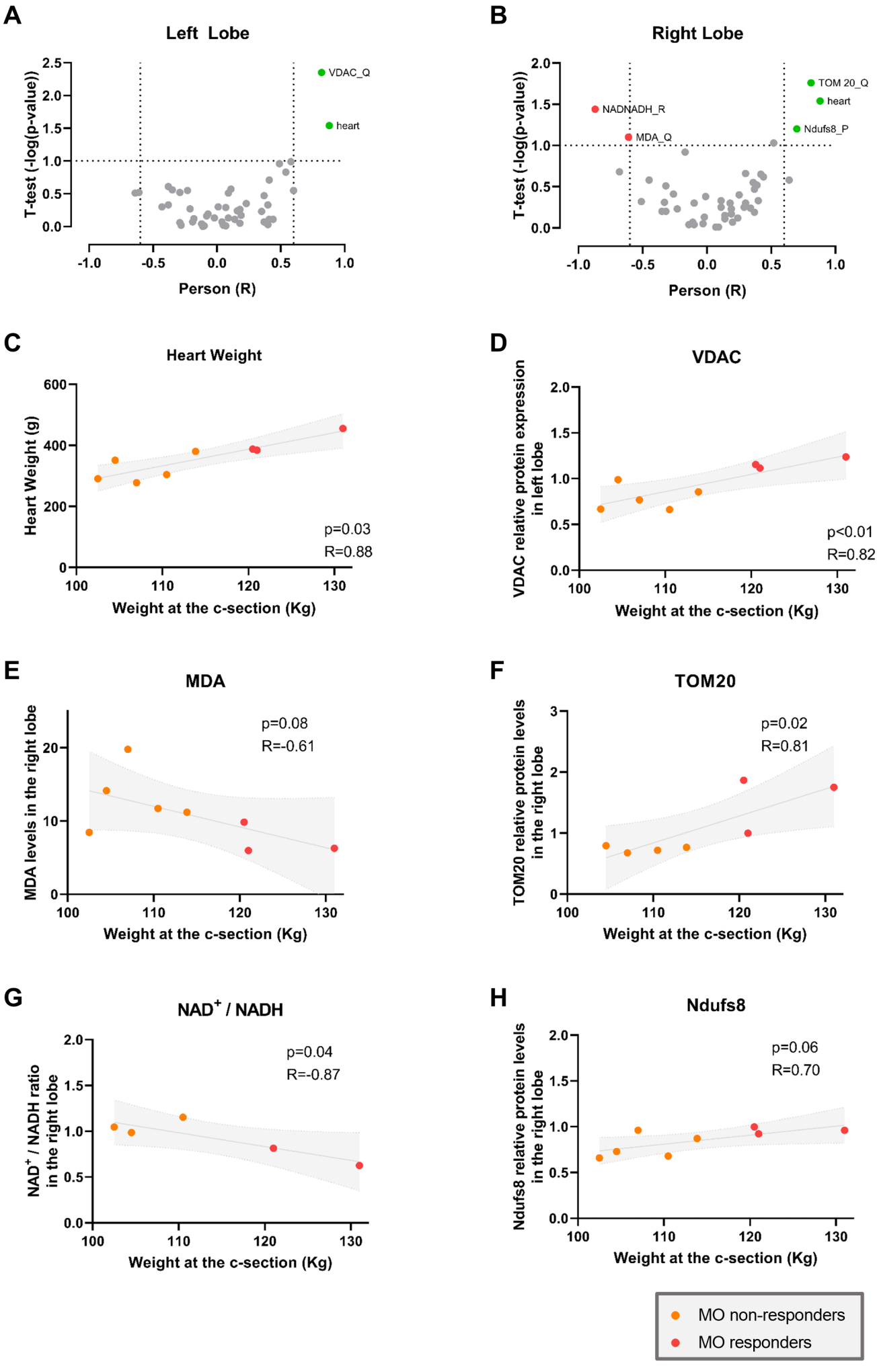
A
Left Lobe
T-test (-log(p-value))
Person (R)
VDAC_Q
heart
B
Right Lobe
T-test (-log(p-value))
Person (R)
NADNADH_R
MDA_Q
TOM 20_Q
heart
Ndufs8_P
C
Heart Weight
Heart Weight (g)
Weight at the c-section (Kg)
p=0.03
R=0.88
D
VDAC
VDAC relative protein expression in left lobe
Weight at the c-section (Kg)
p<0.01
R=0.82
E
MDA
MDA levels in the right lobe
Weight at the c-section (Kg)
p=0.08
R=-0.61
F
TOM20
TOM20 relative protein levels in the right lobe
Weight at the c-section (Kg)
p=0.02
R=0.81
G
NAD+ / NADH
NAD+ / NADH ratio in the right lobe
Weight at the c-section (Kg)
p=0.04
R=-0.87
H
Ndufs8
Ndufs8 relative protein levels in the right lobe
Weight at the c-section (Kg)
p=0.06
R=0.70
MO non-responders
MO responders